

Relativistic flying laser focus by a laser-produced parabolic plasma mirrorTae Moon Jeong^{Ⓧ,*}, Sergei V. Bulanov,[†] Petr Valenta^{Ⓧ,‡} and Georg Korn*Institute of Physics of the ASCR, ELI-Beamlines, Na Slovance 2, 18221 Prague, Czech Republic*Timur Zh. Esirkepov, James K. Koga[Ⓧ], Alexander S. Pirozhkov[Ⓧ], and Masaki Kando[Ⓧ]*Kansai Photon Science Institute, National Institutes for Quantum Science and Technology,
8-1-7 Umemidai, Kizugawa-shi, Kyoto 619-0215, Japan*

Stepan S. Bulanov

Lawrence Berkeley National Laboratory, Berkeley, California 94720, USA

(Received 22 March 2021; revised 31 August 2021; accepted 8 November 2021; published 30 November 2021)

The question of electromagnetic field intensification towards the values typical for strong field quantum electrodynamics is of fundamental importance. One of the most promising intensification schemes is based on the relativistic-flying mirror concept, which shows that the electromagnetic radiation reflected by the mirror will be frequency upshifted by a factor of $4\gamma^2$ (γ is the Lorentz factor of the mirror). In laser-plasma interactions, such a mirror travels with relativistic velocities through plasma and typically has a parabolic form, which is advantageous for light intensification. Thus, a relativistic-flying parabolic mirror reflects the counterpropagating radiation in the form of a focused and flying electromagnetic wave with a high frequency. The relativistic-flying motion of the laser focus makes the electric and magnetic field distributions of the focus complicated, and the mathematical expressions describing the field distributions of the focus become of fundamental interest. We present analytical expressions describing the field distribution formed by an ideal flying mirror which has a perfect reflectance over the entire surface and wavelength range. The peak field strength of an incident laser pulse with a center wavelength of λ_0 and an effective beam radius of w_e is enhanced by a factor proportional to $\gamma^3(w_e/\lambda_0)$ in the relativistic limit. Electron-positron pair production is investigated in the context of invariant fields based on the enhanced electromagnetic field. The pair production rate under the relativistic-flying laser focus is modified by the Lorentz γ -factor and the beam radius-wavelength ratio (w_e/λ_0). We show that the electron-positron pairs can be created by colliding two counterpropagating relativistic-flying laser focuses in vacuum, each of which is formed when a 180 TW laser pulse is reflected by a relativistic-flying parabolic mirror with $\gamma = 12.2$.

DOI: [10.1103/PhysRevA.104.053533](https://doi.org/10.1103/PhysRevA.104.053533)**I. INTRODUCTION**

As femtosecond high-power laser technology advances [1–3], the acceleration of charged particles and the generation of high-energy photons using high-power laser pulses have been extensively investigated [4–6]. Much attention has been recently paid to the quantum electrodynamic (QED) phenomena under an ultrastrong laser field (known as the strong field QED (SF QED) [7–9]), including vacuum birefringence [10–13], photon-photon scattering [14–21], and electron-positron pair production via the Schwinger mechanics [22–25]. An ultrahigh laser intensity close to the Schwinger intensity (10^{29} W/cm²) is desirable for the QED study. Therefore, international efforts constructing a high-power laser facility having a 100 PW, or even higher power

to EW, power level have recently been initiated [26–29]. However, due to the very low probability for the QED event with the currently available laser power, various sophisticated focusing schemes, such as multiple beam focusing [23], tight focusing (including λ^3 focusing idea) [30,31], and 4π -spherical focusing [32,33] schemes, are proposed to maximize the laser field strength in the focal plane at a given laser power.

Since the QED event probability depends on the quantum nonlinearity parameter χ_e , defined as $\sqrt{|(F^{\mu\nu}p_\nu)^2|}/mcE_{\text{Sch}}$ [34], an approach to observe the QED phenomena with a relatively lower laser power is to use ultrarelativistic particles interacting with the laser field [16,35–39]. Here, $F^{\mu\nu}$ is the electromagnetic field tensor, p_ν the momentum of the ultrarelativistic particle, and E_{Sch} the Schwinger field, $m^2c^3/e\hbar$. Using the expression for the parameter χ_e for describing the QED processes, one can say that when $\chi_e > 1$ in the electron rest frame, the electric field exceeds the Schwinger limit. Another interesting approach, instead of using ultrarelativistic particles, is to use the laser field reflected from a relativistic flying mirror (RFM) [40,41]. In this case, the laser field reflected by the RFM experiences the double Doppler effect [42], and its angular frequency and field strength are enhanced

*taemoon.jeong@eli-beams.eu

†Also at Kansai Photon Science Institute, National Institutes for Quantum Science and Technology, 8-1-7 Umemidai, Kizugawa-shi, Kyoto 619-0215, Japan.

‡Also at Faculty of Nuclear Sciences and Physical Engineering, Czech Technical University in Prague, Brehova 7, 11519 Prague, Czech Republic.

by a factor of $4\gamma^2$ in the relativistic limit of $\beta \rightarrow 1$. In [43], it is demonstrated through particle-in-cell simulations that the focused intensity of the reflected laser pulse can exceed the conventionally focused laser intensity when a counterpropagating laser pulse is focused by a relativistic-flying parabolic mirror (RFPM).

Due to the relativistic motion of the RFPM, the laser pulse focused by the RFPM travels with a relativistic speed as well, providing the relativistic-flying laser focus (RLF) and opening new regimes for SF QED studies [44]. However, despite many interesting features introduced in [45–49], it is not yet clear exactly how the electromagnetic (EM) field of the RLF is distributed and propagates in time and space. Thus, it is of fundamental interest to obtain mathematical expressions describing the EM field distribution of the RLF and to apply the ultrastrong field for the study of the SF-QED occurring in a very small spacetime region. We should note that another concept of flying focus generated by a chromatic focusing of chirped laser pulses was recently introduced and received considerable interest [50].

In this paper, we present mathematical formulas describing three-dimensional field distributions of the RLF focused by a RFPM. When deriving the mathematical formulas for the field of RLF, two frames of reference are employed: one is the laboratory frame of reference (hereafter, laboratory frame) and the other is the boosted frame of reference (hereafter, boost frame) which moves with the RLF. An incoming laser pulse in the laboratory frame is reexpressed in the boost frame through the Lorentz transformation. Then, a focused field is calculated in the boost frame through the diffraction integral. The 4π -spherical focusing scheme [33] is applied to calculate the focused field since the f -number defined as the focal length divided by the beam size becomes $\ll 1$ in the boost frame. A radially or azimuthally polarized [transverse magnetic (TM) or transverse electric (TE) mode] EM wave [51] with a proper apodization function is assumed for an analytical mathematical expression under the 4π -spherically focusing scheme. The focused field distribution in the boost frame is again Lorentz transformed to reveal the flying characteristics of the field distribution of the RLF in the laboratory frame.

The paper is organized as follows: The change in optical characteristics, such as wavelength, pulse duration, and field strength, of a laser pulse reflected by a relativistic-flying flat mirror (RFFM) are briefly reviewed in Sec. II. In Sec. III, the mathematical formulas expressing the field distribution of the RLF reflected and focused by an RFPM are derived and discussed. The invariant fields based on Poincaré invariants (\mathcal{F} and \mathcal{G}) are calculated and used to find the pair production rate via the Schwinger mechanism [22,52]. The electron-positron pair production as an example of QED phenomena is investigated with field expressions of RLF in Sec. IV.

II. LASER PULSE REFLECTED BY THE RELATIVISTIC-FLYING FLAT MIRROR

Let us first consider that a linearly polarized (x -polarized) incident laser pulse is reflected by a RFFM traveling along the $+z$ axis with a speed of v (or $\beta = v/c$), where c is the speed of light (see Fig. 1). In a laboratory frame [\mathcal{L}_1 , $x^\mu = (ct, -x, -y, -z)$], before the reflection, the laser pulse prop-

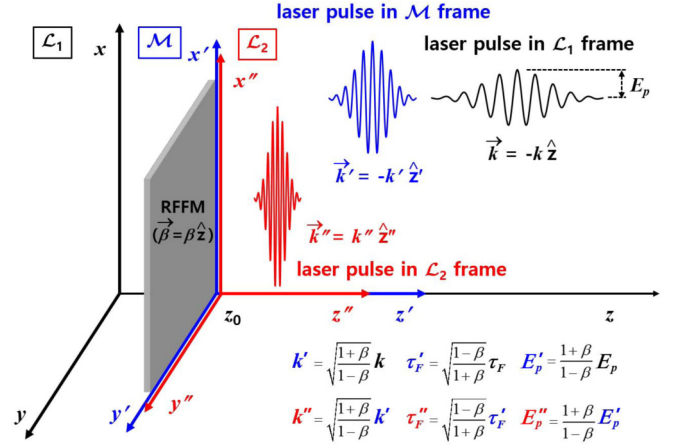


FIG. 1. Laser pulse reflected by a relativistic-flying flat mirror (RFFM). Due to the double Doppler effect, the wave vector k and the E-field strength E_p in time are enhanced by a total factor of $(1 + \beta)/(1 - \beta)$ and the pulse duration τ_F is shortened by a total factor of $(1 - \beta)/(1 + \beta)$.

agating along the $-z$ axis ($\vec{k} = -k\hat{z} = -\omega/c\hat{z}$) is expressed as

$$\begin{aligned} E(x, y, z; t) &= \int_{-\infty}^{\infty} E_0(x, y; \omega) e^{i\omega(t+z/c)} d\omega \\ &= E_0(x, y) \int_{-\infty}^{\infty} G(\omega) e^{i\omega(t+z/c)} d\omega \\ &= E_p(x, y) e^{-(t+z/c)^2/2\tau_G^2} e^{i\omega_0(t+z/c)}. \end{aligned} \quad (1)$$

Here, $E_0(x, y; \omega) = E_0(x, y)G(\omega)$. A Gaussian spectrum, $G(\omega) = \exp[-(\omega - \omega_0)^2/2\Delta\omega^2]$, is assumed for the laser pulse with a center frequency of ω_0 and a Gaussian width ($\Delta\omega$) of the spectrum. $E_0(x, y; \omega)$ and $E_p(x, y)$ are peak field strengths in spectral and time domains, respectively. The peak field strength $E_p(x, y)$ in time is represented by $\sqrt{2\pi}\Delta\omega E_0(x, y)$ and the Gaussian width in time, τ_G , by $1/\Delta\omega$. So, the peak intensity \mathcal{I}_p in time can be calculated as $\Delta\omega^2 \mathcal{I}(\omega)$, with $\mathcal{I}(\omega) = c\epsilon_0 E_0(x, y)/2$. It should be noted that the spectral bandwidth $\Delta\omega_F$ and pulse duration τ_F at full width at half maximum (FWHM) are given by $2\sqrt{\ln 2}\Delta\omega$ and $2\sqrt{\ln 2}\tau_G$, respectively. For the flat-top spatial beam profile [$E_0(x, y) = E_0$] with a radius of r_0 , the energy density $\mathcal{E}_D(t)$ and the total laser pulse energy \mathcal{E}_T are given by $(1/2)\epsilon_0 E_p^2 \exp[-(t+z/c)^2/\tau_G^2]$ and $(\sqrt{\pi}/2)\epsilon_0 A c \tau_G E_p^2$, respectively. Here, A is the beam area given by πr_0^2 . For the Gaussian [$\exp(-r^2/2w_0^2)$] and lowest-order Laguerre-Gaussian [$(r/w_0) \exp(-r^2/2w_0^2)$] beam profiles, the area A should be replaced by the effective area, $A_e = \pi w_e^2$, where w_e is w_0 for the Gaussian beam and $w_0\sqrt{2p+m+1}$ for the p th radial, m th azimuthal Laguerre-Gaussian beam. Now, the intensity \mathcal{I} of the laser pulse defined as $\mathcal{E}_T/A_{\text{eff}}\tau_G$ becomes $(\sqrt{\pi}/2)\epsilon_0 c E_p^2$.

The same laser pulse can be expressed in the boost frame [\mathcal{M} , $x'^\mu = (ct', -x', -y', z')$] by using the Lorentz transformation. Through the Lorentz transformation, the four-vector

x'^{μ} and the E-field components in the boost frame are expressed as

$$\begin{aligned} ct' &= \gamma(ct - \beta z), \quad x' = x, \\ y' &= y, \quad z' = \gamma(z - \beta ct), \\ \vec{E}'_{\perp}(x', y'; \omega) &= \gamma[\vec{E}_{\perp}(x, y; \omega) + c\vec{\beta} \times \vec{B}(x, y; \omega)], \end{aligned} \quad (2a)$$

and

$$\vec{E}'_{\parallel}(x', y'; \omega) = \vec{E}_{\parallel}(x, y; \omega). \quad (2c)$$

Here, the Lorentz γ -factor is defined as $1/\sqrt{1-\beta^2}$. The subscripts \perp and \parallel refer to the polarization components perpendicular and parallel to the mirror traveling direction (+z), respectively. Since the incident laser pulse is x-polarized, $\vec{E}(x, y; \omega) = \hat{x}E_0(x, y; \omega)$ and $\vec{B}(x, y; \omega) = -\hat{y}B_0(x, y; \omega)$. The E-field $E'(x', y', z'; t')$ in time in the boost frame can be obtained by the Fourier transformation of $E(x', y'; \omega)$ in the ω domain as

$$\begin{aligned} E'(x', y', z'; t') &= \gamma \int_{-\infty}^{\infty} [E_0(x, y; \omega) + c\beta B_0(x, y; \omega)] e^{i\omega(t+z/c)} d\omega \\ &= \sqrt{\frac{1+\beta}{1-\beta}} E_0(x, y) \int_{-\infty}^{\infty} G(\omega) e^{i\omega(t+z/c)} d\omega, \end{aligned} \quad (3)$$

with $E_0 = cB_0$. Then, using the Lorentz transformation given by Eq. (2a), we obtain

$$\begin{aligned} E'(x', y', z'; t') &= \sqrt{\frac{1+\beta}{1-\beta}} E_0(x', y') \int_{-\infty}^{\infty} G(\omega) e^{i\sqrt{\frac{1+\beta}{1-\beta}}\omega(t'+z'/c)} d\omega \\ &= E_0(x', y') \int_{-\infty}^{\infty} G(\omega') e^{i\omega'(t'+z'/c)} d\omega' \\ &= E'_p(x', y') e^{-(t'+z'/c)^2/2\tau_G'^2} e^{i\omega'_0(t'+z'/c)}. \end{aligned} \quad (4)$$

In Eq. (4), a new angular frequency ω' , defined as $\sqrt{(1+\beta)/(1-\beta)}\omega$, is introduced in the boost frame. Then, the Gaussian spectrum $G(\omega)$ is modified as $G(\omega') = \exp[-(\omega' - \omega'_0)^2/2(\Delta\omega')^2]$ with a new center frequency ω'_0 [$=\sqrt{(1+\beta)/(1-\beta)}\omega_0$] and spectral bandwidth $\Delta\omega'$ [$=\Delta\omega\sqrt{(1+\beta)/(1-\beta)}$]. The peak field strength $E'_p(x', y')$ [$=\sqrt{2\pi}\Delta\omega' E_0(x', y')$] in the boost frame is enhanced by a factor of $\sqrt{(1+\beta)/(1-\beta)}$ since $E_0(x', y') = E_0(x, y)$. The Gaussian width in time, $\tau_G' (= 1/\Delta\omega')$, is reduced by a factor of $\sqrt{(1+\beta)/(1-\beta)}$. After straightforward calculations, the following relationships for the total energy \mathcal{E}'_T and the intensity \mathcal{I}' of the laser pulse can be obtained:

$$\mathcal{E}'_T = \sqrt{\frac{1+\beta}{1-\beta}} \mathcal{E}_T \quad \text{and} \quad \mathcal{I}' = \frac{1+\beta}{1-\beta} \mathcal{I}. \quad (5)$$

Next, the incident laser pulse experiences the reflection by the RFFM in the boost frame. The origin of the boost frame is located at $(0, 0, z_0)$ in the laboratory frame. After the reflection in the boost frame, the propagation direction of the wave vector of the incident laser pulse is reversed ($\vec{k}' = k'\hat{z} = \omega'/c\hat{z}$). In this case, the incident laser pulse has the E-field

$\vec{E}'_0(x', y'; \omega') = \hat{x}E'_0(x', y'; \omega')$ and the B-field $\vec{B}'_0(x', y'; \omega') = \hat{y}B'_0(x', y'; \omega')$. Then, from Eq. (4), the E-field of the reflected pulse is given by

$$\begin{aligned} E'_r(x', y', z'; t') &= E_0(x', y') \int_{-\infty}^{\infty} G(\omega') e^{i\omega'(t'-z'/c)} d\omega' \\ &= \int_{-\infty}^{\infty} E'(x', y'; \omega') e^{i\omega'(t'-z'/c)} d\omega'. \end{aligned} \quad (6)$$

The Lorentz transformations between the boost frame and another laboratory frame [\mathcal{L}_2 , $x''^{\mu} = (ct'', -x'', -y'', -z'')$], of which the origin coincides with the boost frame, relate the four-vector and the field components as

$$\begin{aligned} ct'' &= \gamma(ct' + \beta z'), \quad x'' = x', \\ y'' &= y', \quad z'' = \gamma(z' + \beta ct'), \end{aligned} \quad (7a)$$

$$\vec{E}''_{\perp}(x'', y''; \omega'') = \gamma[\vec{E}'_{\perp}(x', y'; \omega') - c\vec{\beta} \times \vec{B}'(x', y'; \omega')], \quad (7b)$$

and

$$\vec{E}''_{\parallel}(x'', y''; \omega'') = \vec{E}'_{\parallel}(x', y'; \omega'). \quad (7c)$$

Again, by performing the Fourier transformation into Eq. (7b) in the ω' domain, we obtain

$$\begin{aligned} E''_r(x'', y'', z''; t'') &= \sqrt{\frac{1+\beta}{1-\beta}} E_0(x'', y'') \int_{-\infty}^{\infty} G(\omega'') e^{i\sqrt{\frac{1+\beta}{1-\beta}}\omega''(t''-z''/c)} d\omega'' \\ &= E_0(x'', y'') \int_{-\infty}^{\infty} G(\omega'') e^{i\omega''(t''-z''/c)} d\omega'' \\ &= E''_p(x'', y'') e^{-(t''-z''/c)^2/2\tau_G''^2} e^{i\omega''_0(t''-z''/c)}. \end{aligned} \quad (8)$$

Here, new angular frequency ω'' , defined as $\sqrt{(1+\beta)/(1-\beta)}\omega' = [(1+\beta)/(1-\beta)]\omega$ in the laboratory frame (\mathcal{L}_2), is introduced. So, the new center frequency ω''_0 and spectral bandwidth $\Delta\omega''$ of $G(\omega'')$ in the laboratory frame (\mathcal{L}_2) are given by

$$\omega''_0 = \frac{1+\beta}{1-\beta}\omega_0 \quad \text{and} \quad \Delta\omega'' = \frac{1+\beta}{1-\beta}\Delta\omega, \quad (9)$$

respectively. From Eq. (8), the peak field strength $E''_p(x'', y'')$ in time is again given by $\sqrt{2\pi}\Delta\omega'' E_0(x, y)$ with $E_0(x'', y'') = E_0(x, y)$, yielding

$$E''_p(x'', y'') = \frac{1+\beta}{1-\beta} E_p(x, y). \quad (10)$$

The Gaussian width in time, τ_G'' , is reduced to $1/\Delta\omega'' = [(1-\beta)/(1+\beta)]\tau_G$. Since $t'' = t$, $x'' = x$, $y'' = y$, and $z'' = z - z_0$, Eq. (8) can be explicitly rewritten in the original laboratory frame (\mathcal{L}_1) as

$$\begin{aligned} E''_r(t) &= \frac{1+\beta}{1-\beta} E_p(x, y) \exp\left[i\frac{1+\beta}{1-\beta}\omega_0\left(t - \frac{z-z_0}{c}\right)\right] \\ &\quad \times \exp\left[-\left(\frac{1+\beta}{1-\beta}\right)^2 \frac{1}{\tau_G^2} \left(t - \frac{z-z_0}{c}\right)^2\right]. \end{aligned} \quad (11)$$

Equation (11) presents several interesting features of the laser pulse reflected from the RFFM. First, the angular frequency of

the reflected pulse is enhanced by a factor of $(1 + \beta)/(1 - \beta)$. For instance, the center wavelength ($\lambda_0 = 0.8 \mu\text{m}$ or 1.55 eV) of the typical PW-class Ti:sapphire laser can be shortened to 1.24 nm (1 keV) when the Lorentz γ -factor of 12.7 [$(1 + \beta)/(1 - \beta) \approx 645$] is considered. Second, the pulse duration τ_F' of the reflected pulse is shortened as $[(1 - \beta)/(1 + \beta)]\tau_F$. Considering a γ -factor of 12.7 again, the pulse duration of 30 fs , which is the typical pulse duration of the PW-class Ti:sapphire laser pulse, can be reduced to 47 as . Thus, the relativistic-flying mirror with a high γ -factor can be a promising plasma optic to produce an attosecond x-ray source [53].

The total energy \mathcal{E}_T'' of the reflected pulse becomes $[(1 + \beta)/(1 - \beta)]\mathcal{E}_T$ and its intensity \mathcal{I}'' is calculated to be $[(1 + \beta)/(1 - \beta)]^2\mathcal{I}$. Thus, the total energy and the intensity of a laser pulse reflected by a RFFM are proportional to $(2\gamma)^2$ and $(2\gamma)^4$ in the relativistic limit. These basic characteristics of a laser pulse reflected by a RFFM seem very striking since the intensity monotonically increases with the Lorentz γ -factor of the RFM and a high E-field strength above the Schwinger field is expected with a high γ -factor. However, considering that the RFM is formed by a driver laser pulse and acquires energy from the driver pulse, the total energy of the reflected pulse can be limited by the total energy \mathcal{E}_{DL} of the driver pulse. This consideration restricts the total energy of the reflected pulse as

$$\mathcal{E}_T'' = \frac{1 + \beta}{1 - \beta}\mathcal{E}_T \leq \mathcal{E}_{DL}, \quad (12)$$

and the highest laser intensity obtained from the RFFM is limited by $[(1 + \beta)(1 - \beta)]\mathcal{E}_{DL}/A\tau_G$ when the energy of the driver laser pulse is less than \mathcal{E}_T'' . In this case, the benefit in the intensity enhancement by the RFFM comes from the contraction in the pulse duration. Although the intensity of the laser pulse reflected by the flying flat mirror is already enhanced by a factor of γ^4 under $\mathcal{E}_{DL} \geq \mathcal{E}_T''$, the laser focus formed by an ideal RFFM provides an additional enhancement factor (compared to the flat mirror case) related to the effect of a frequency upshift by the double Doppler effect, so it is still of fundamental interest to derive the field expressions for the laser focus reflected by an ideal RFFM.

III. LASER PULSE REFLECTED BY THE RELATIVISTIC-FLYING PARABOLIC MIRROR

Even though the RFFM helps one understand the basic properties of the reflected field, the RFFM is a more realistic plasma mirror encountered when a fs high-power laser propagates through the underdense plasma medium. A strong laser pulse (of which the normalized vector potential a_0 is above unity) propagating in the plasma pushes electrons through the ponderomotive force to form a plasma cavity, and electrons return back by the recoiling force and form a high-density electron layer on the backside of the cavity. The shape of the electron layer is close to a paraboloid [48,54,55] and, due to the high-electron density, the electron layer behaves like a parabolic mirror. Since the plasma cavity moves with a relativistic speed, the high-density electron layer forms the RFFM. A counterpropagating laser pulse is reflected and focused by the RFFM. The reflected pulse experiences the frequency upshift and the shortening of pulse duration due to

the double Doppler effect as discussed in the previous section, and its focus also moves with a relativistic speed. And, when the incident laser pulse is reflected by the RFFM, due to the relativistic effect it also experiences a different curvature for the RFFM from the nominal curvature in the laboratory. Finally, all these effects related to the relativistic motion should be properly considered in calculating the field distribution of the RLF. In this work, we consider only a constantly moving mirror in the optimal regime.

A. Focal length of the RFFM

Now, in order to describe how the curvature and the focal length of the mirror change by the relativistic effect, let us first consider the equation for the surface of the RFFM. The unprimed and primed four-vectors, such as $x^\mu = (ct, -x, -y, -z)$ and $x'^\mu = (ct', -x', -y', -z')$, are used for describing coordinates in the laboratory frame (\mathcal{L}_1) and the boost frame (\mathcal{M}), respectively (see Fig. 2). Assuming that the focus and the vertex of the RFFM are located at the origin and $-f'$ on the z' axis, the equation of the surface for the parabolic mirror is expressed in the boost frame as

$$z' = \frac{x'^2 + y'^2}{4f'} - f', \quad (13)$$

where f' is known as the focal length of the RFFM. For the nonrelativistic case, Eq. (13) can be obtained by equating two lengths of d'_1 and d'_2 in Fig. 2(b). Here, the lengths of d'_1 and d'_2 are given by $z' + 2f'$ and $\sqrt{x'^2 + y'^2 + z'^2}$, respectively.

For the relativistic case, Eq. (13) is generalized by the Lorentz invariant property of the interval, $x'_\mu x'^\mu$, between two spacetime events given by the four-vector, x'^μ . When an EM wave propagates to an event P from two different events (O and A), as shown in Fig. 2(b), a four-vector between two events [$P = (0, -x', -y', -z')$ and $A = (ct', -x', -y', 2f')$] is expressed by $d''_1 = (ct', 0, 0, 2f' + z')$ and its Lorentz-invariant interval $d''_{1\mu} d''_1{}^\mu$ is given by $c^2 t'^2 - (2f' + z')^2$. The other four-vector between two events [P and $O = (ct', 0, 0, 0)$] is expressed by $d''_2 = (ct', x', y', z')$ and its Lorentz-invariant interval $d''_{2\mu} d''_2{}^\mu$ is $c^2 t'^2 - x'^2 - y'^2 - z'^2$. Since the RFFM moves along the $+z$ axis, the Lorentz transformations between the laboratory and the boost frames are given as

$$ct' = \gamma(ct - \beta z), \quad x' = x, \quad y' = y, \quad (14a)$$

and

$$z' = \gamma(z - \beta ct). \quad (14b)$$

Now, by equating the two intervals $d''_{1\mu} d''_1{}^\mu$ and $d''_{2\mu} d''_2{}^\mu$, we obtain the equation for the surface of the RFFM in the laboratory frame as

$$z = \frac{x^2 + y^2}{4\gamma f'} - \gamma f' + \frac{\gamma^2 - 1}{\gamma} f' + \beta ct. \quad (15)$$

In the nonrelativistic limit ($\gamma \rightarrow 1$ and $\beta \rightarrow 0$), Eq. (15) reduces to Eq. (13). Equation (15) provides useful information on how the RFFM behaves with an incident laser pulse. First, the surface of the RFFM is described by the equation $z = (x^2 + y^2)/4\gamma f'$ in the laboratory frame. This means that

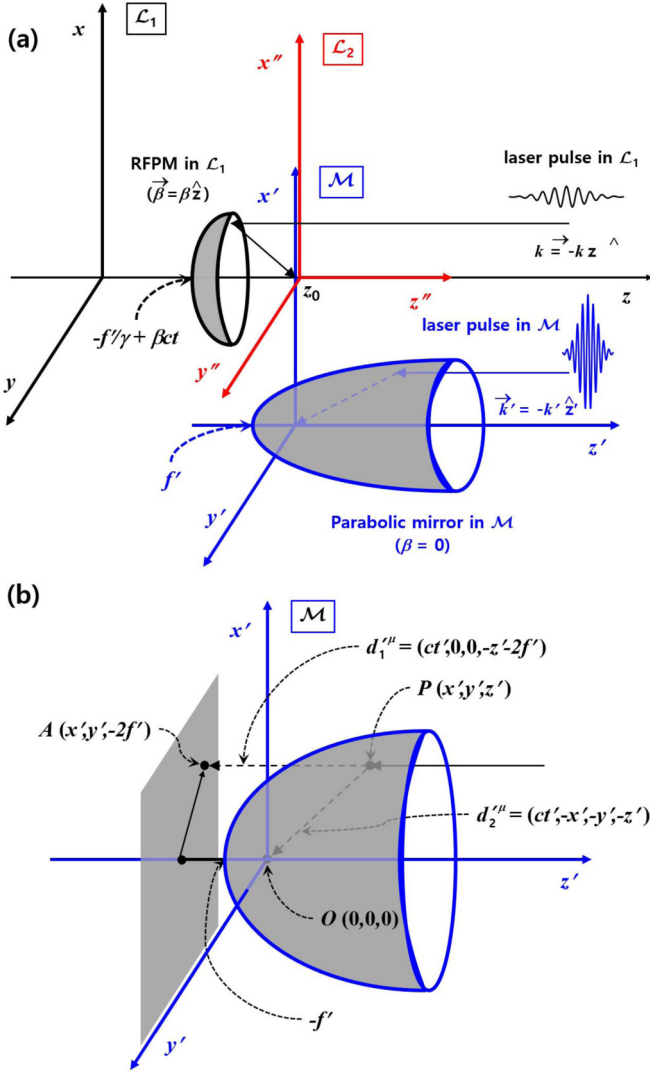


FIG. 2. Relativistic-flying parabolic mirror (RFPM) in the laboratory and the boost frames. (a) The shape of the parabolic mirror is elongated in the boost frame (\mathcal{M}) and the focal length becomes short by a factor of γ in the boost frame. (b) The surface equation of the paraboloid in the boost frame can be obtained from the invariant property of event intervals, $d'_{1\mu}d'_{1\mu}$ and $d'_{2\mu}d'_{2\mu}$.

the nominal focal length ($\gamma f'$) of the RFPM in the laboratory frame is γ times longer than that (f') in the boost frame [19]. An intense ($a_0 = 3$) fs laser pulse propagating in a plasma medium produces a RFPM and its focal length ($\gamma f'$) observed in the laboratory frame is about $2 \mu\text{m}$. This means that in the boost frame, the focal length (f') of the RFPM becomes as short as $0.1 \mu\text{m}$ with a Lorentz factor of $\gamma = 20$. This is contrary to the length contraction which is well known in the special theory of relativity. The change in the focal length in the boost frame alters the focusing condition to the 4π -spherical focusing scheme. For instance, the f -number (defined as the focal length divided by the beam size) changes from 0.2 to 0.01, assuming an incident beam size of $\sim 10 \mu\text{m}$. Thus, the field distribution of the laser focus in the boost frame should be calculated under the 4π -spherical focusing condition. Second, the vertex of the RFPM is located on

$\gamma f' + (\gamma^2 - 1)f'/\gamma + \beta ct$ at a certain time t , and its position moves with a relativistic speed of βc in the laboratory frame. As a result, the laser focus moves with a relativistic speed of βc in the laboratory frame as well.

For simplicity, instead of directly calculating the field distribution of the RLF in the laboratory frame, we calculate the focused field distribution first in the boost frame, and then convert it in the laboratory frame through the Lorentz transformation.

B. Focused field in the boost frame

Since the incident E-field in the boost frame is expressed by the Fourier transformation as in Eq. (4), a monochromatic laser field $E'(x', y'; \omega')$ in the boost frame is given by

$$E'(x', y'; \omega') = E_0(x, y)G(\omega')e^{i\omega'(z'/c)}. \quad (16)$$

This laser field is focused by the RFPM to form a field distribution under the 4π -spherical focusing scheme in the boost frame. In this study, we assume that the incident laser pulse is radially polarized (TM mode) or azimuthally polarized (TE mode), since analytic solutions for those fields exist under the 4π -spherically focusing condition with a specific apodization function. According to [33], in the boost frame (\mathcal{M}), the electric and magnetic fields of the 4π -spherically focused monochromatic TM mode EM wave are expressed as

$$\begin{aligned} \vec{E}'_f(\rho', \theta'; \omega') &= \hat{\theta}' i E'_p(\omega') a(\rho', \theta'; \omega') e^{i\omega' t'} \\ &= \vec{E}'_{f,\perp} + \vec{E}'_{f,\parallel} \end{aligned} \quad (17a)$$

and

$$\begin{aligned} \vec{B}'_f(\rho', \theta'; \omega') &= -\hat{\phi}' B'_p(\omega') b(\rho', \theta'; \omega') e^{i\omega' t'} \\ &= \vec{B}'_{f,\parallel}. \end{aligned} \quad (17b)$$

Here, $\rho' (= \sqrt{x'^2 + y'^2 + z'^2})$ is the magnitude of the radial displacement vector, $\vec{\rho}' = \hat{\rho}' \rho' = \hat{x}x' + \hat{y}y' + \hat{z}z'$, from the origin to an observation point (x', y', z') near the origin, and θ' is the polar angle defined as $\cos^{-1}(z'/\rho')$. Again, the angular frequency ω' in the boost frame is given by $\sqrt{(1+\beta)/(1-\beta)}\omega$ and the Gaussian spectrum in Eq. (4) is assumed. The peak field strength $E'_p(\omega')$ at the focus at a certain frequency ω' is given by $(\pi/2)k'\rho'_S E'_S(\omega')$. The E-field $E'_S(\omega')$ on a virtual sphere with a radius of ρ'_S is related to the incident laser power [$P'_L(\omega') = (1/2)c\epsilon_0 E'^2(x', y'; \omega')A_e$] as $\sqrt{3P'_L(\omega')/4\pi c\epsilon_0(\rho'_S)^2}$ (see Eq. (35) in [33]). Thus, the peak field strength $E'_p(\omega')$ is calculated to be

$$\begin{aligned} E'_p(\omega') &= \frac{k'}{4} \sqrt{\frac{3\pi A_e}{2}} E_0(x, y) G(\omega') \\ &= \frac{k'}{4} \sqrt{\frac{3\pi A_e \mathcal{I}}{c\epsilon_0}} G(\omega') \\ &= C_f \mathcal{I}^{1/2} \frac{k'}{4} G(\omega'), \end{aligned} \quad (18)$$

where C_f is a constant $\sqrt{3\pi A_e/c\epsilon_0} = \sqrt{3/c\epsilon_0\pi} w_e$ related to the effective radius w_e , and $k' (= \omega'/c)$ is the magnitude of the wave vector, $\vec{k}' = \hat{\rho}' k'$, originating from the origin in the

boost frame. The laser intensity \mathcal{I} in the laboratory frame is given by $(1/2)c\epsilon_0 E_0^2(x, y)$.

The spatial distribution functions $a(\rho', \theta'; \omega')$ and $b(\rho', \theta'; \omega')$ in Eq. (17) are expressed with the n th-order spherical Bessel function of the first kind, $j_n(\cdot)$, and the Legendre and associated Legendre functions, $P_n(\cdot)$ and $P_n^m(\cdot)$, as

$$a(\rho', \theta'; \omega') = j_0\left(\frac{\omega'}{c}\rho'\right) + \frac{5}{2^3}j_2\left(\frac{\omega'}{c}\rho'\right)P_2(\cos\theta') + \dots \quad (19a)$$

and

$$b(\rho', \theta'; \omega') = \frac{4}{\pi}j_1\left(\frac{\omega'}{c}\rho'\right)P_1^1(\cos\theta'). \quad (19b)$$

In Eq. (19), the argument $k'\rho'$ ($= \vec{k}' \cdot \vec{\rho}'$) in spherical coordinates is replaced by $(\omega'/c)\rho'$. So, $k'\rho'$ [or $(\omega'/c)\rho'$] can be expressed as $k'_x x' + k'_y y' + k'_z z'$ in Cartesian coordinates. Since the above field distributions propagate along the z axis in \mathcal{L}_1 , it is convenient to express Eq. (17) in Cartesian coordinates before performing the Lorentz transformation. The unit vectors $\hat{\theta}'$ and $\hat{\phi}'$ in spherical coordinates of the boost frame are expressed as $\hat{\theta}' = \cos\theta' \cos\phi' \hat{x}' + \cos\theta' \sin\phi' \hat{y}' - \sin\theta' \hat{z}'$ and $\hat{\phi}' = \sin\phi' \hat{x}' - \cos\phi' \hat{y}'$ in Cartesian coordinates; then we rewrite Eq. (17) as

$$\begin{bmatrix} E'_{f,x'} \\ E'_{f,y'} \\ E'_{f,z'} \end{bmatrix} = iE'_p(\omega')a(\rho', \theta'; \omega')e^{i\omega't'} \begin{bmatrix} \cos\theta' \cos\phi' \\ \cos\theta' \sin\phi' \\ -\sin\theta' \end{bmatrix} \quad (20a)$$

and

$$\begin{bmatrix} B'_{f,x'} \\ B'_{f,y'} \\ B'_{f,z'} \end{bmatrix} = -B'_p(\omega')b(\rho', \theta'; \omega')e^{i\omega't'} \begin{bmatrix} \sin\phi' \\ -\cos\phi' \\ 0 \end{bmatrix}. \quad (20b)$$

The electric and magnetic fields in Eq. (20) consist of incoming ($t' + \rho'/c$) and outgoing ($t' - \rho'/c$) field components. The spatial distribution function $a(\rho', \theta'; \omega')$ in the electric field can be approximated as $j_0(\omega'\rho'/c)$; then, $a(\rho', \theta'; \omega')e^{i\omega't'}$ and $b(\rho', \theta'; \omega')e^{i\omega't'}$ can be separated by two parts as

$$a(\rho', \theta'; \omega')e^{i\omega't'} = (a_+ + a_-)e^{i\omega't'} \quad (21a)$$

and

$$b(\rho', \theta'; \omega')e^{i\omega't'} = (b_+ + b_-) \sin\theta' e^{i\omega't'}, \quad (21b)$$

where incoming (a_+ and b_+) and outgoing (a_- and b_-) field components are given by

$$a_+ = \frac{e^{i\omega'\rho'/c}}{2i\omega'\rho'/c}, \quad a_- = -\frac{e^{-i\omega'\rho'/c}}{2i\omega'\rho'/c}, \quad (22a)$$

$$b_+ = \frac{4}{\pi} \left[\frac{e^{i\omega'\rho'/c}}{2i(\omega'\rho'/c)^2} - \frac{e^{i\omega'\rho'/c}}{2\omega'\rho'/c} \right], \quad (22b)$$

and

$$b_- = \frac{4}{\pi} \left[-\frac{e^{-i\omega'\rho'/c}}{2i(\omega'\rho'/c)^2} - \frac{e^{-i\omega'\rho'/c}}{2\omega'\rho'/c} \right]. \quad (22c)$$

In this section, the electromagnetic field focused by the RFPM is expressed in the boost frame. In the following

sections, the Lorentz transformation of the field into the laboratory frame (\mathcal{L}_2) and the spatiotemporal field distribution in the laboratory frame will be explained.

C. Lorentz transformation for incoming and outgoing fields

For phase factors of incoming and outgoing fields, the Lorentz transformations from the boost frame to the laboratory frame yield

$$\begin{aligned} \omega' \left(t' + \frac{\rho'}{c} \right) &= \omega' t' + k'_x x' + k'_y y' + k'_z z' \\ &= \omega' t \gamma (1 - \beta \cos\theta') + k' x \sin\theta' \cos\phi' \\ &\quad + k' y \sin\theta' \sin\phi' + k' z \gamma (\cos\theta' - \beta) \end{aligned} \quad (23a)$$

and

$$\begin{aligned} \omega' \left(t' - \frac{\rho'}{c} \right) &= \omega' t' - k'_x x' - k'_y y' - k'_z z' \\ &= \omega' t \gamma (1 + \beta \cos\theta') - k' x \sin\theta' \cos\phi' \\ &\quad - k' y \sin\theta' \sin\phi' - k' z \gamma (\cos\theta' + \beta), \end{aligned} \quad (23b)$$

with the expression of $(\omega'/c)\rho' = k'_x x' + k'_y y' + k'_z z'$. By introducing new variables ω'_+ and ω'_- for the angular frequencies of incoming and outgoing fields in the laboratory frame, we define

$$\omega'_+ = \omega' \gamma (1 - \beta \cos\theta'_+) \quad \text{and} \quad \omega'_- = \omega' \gamma (1 + \beta \cos\theta'_-), \quad (24)$$

and obtain the Lorentz-invariant properties for the phase as $\omega'(t' + \rho'/c) = \omega'_+(t + \rho/c)$ and $\omega'(t' - \rho'/c) = \omega'_-(t - \rho/c)$. Here, $+$ and $-$ symbols in the subscript are used to represent incoming and outgoing fields. From the Lorentz invariant properties of the phase, the following relationships between the polar angles for the incoming and outgoing fields are obtained:

$$\sin\theta'_+ = \frac{\sin\theta}{\gamma(1 + \beta \cos\theta)} \quad \text{and} \quad \cos\theta'_+ = \frac{\cos\theta + \beta}{1 + \beta \cos\theta}, \quad (25a)$$

$$\sin\theta'_- = \frac{\sin\theta}{\gamma(1 - \beta \cos\theta)} \quad \text{and} \quad \cos\theta'_- = \frac{\cos\theta - \beta}{1 - \beta \cos\theta}. \quad (25b)$$

And, with the help of Eq. (25), Eq. (23) can be rewritten as

$$\begin{aligned} \omega' \left(t' + \frac{\rho'}{c} \right) &= \frac{\omega' t}{\gamma(1 + \beta \cos\theta)} + \frac{k' x \sin\theta \cos\phi}{\gamma(1 + \beta \cos\theta)} \\ &\quad + \frac{k' y \sin\theta \sin\phi}{\gamma(1 + \beta \cos\theta)} + \frac{k' z \cos\theta}{\gamma(1 + \beta \cos\theta)} \end{aligned} \quad (26a)$$

and

$$\begin{aligned} \omega' \left(t' - \frac{\rho'}{c} \right) &= \frac{\omega' t}{\gamma(1 - \beta \cos\theta)} - \frac{k' x \sin\theta \cos\phi}{\gamma(1 - \beta \cos\theta)} \\ &\quad - \frac{k' y \sin\theta \sin\phi}{\gamma(1 - \beta \cos\theta)} - \frac{k' z \cos\theta}{\gamma(1 - \beta \cos\theta)}. \end{aligned} \quad (26b)$$

So, it is clear that ω''_{\pm} should be expressed as

$$\omega''_{\pm} = \frac{\omega'}{\gamma(1 \pm \beta \cos \theta)} \quad (27)$$

in the laboratory frame. When $\theta = 0$ (+z direction), the angular frequencies for incoming and outgoing fields become $\omega''_{\pm} = [(1 + \beta)/(1 \pm \beta)]\omega$. Now, it is convenient to introduce new variables $\Omega_{1,2}$ and $\Gamma_{1,2}$, defined as

$$\Omega_1 = \frac{\omega'}{\gamma(1 - \beta^2 \cos^2 \theta)}, \quad \Omega_2 = \frac{\omega' \beta \cos \theta}{\gamma(1 - \beta^2 \cos^2 \theta)}, \quad (28a)$$

$$\Gamma_1 = \frac{\omega'/c}{\gamma(1 - \beta^2 \cos^2 \theta)}, \quad \Gamma_2 = \frac{(\omega'/c)\beta \cos \theta}{\gamma(1 - \beta^2 \cos^2 \theta)}. \quad (28b)$$

Then, the phase factors for incoming and outgoing fields can be rewritten as

$$\omega' \left(t' + \frac{\rho'}{c} \right) = (\Omega_1 - \Omega_2)t + (\Gamma_1 - \Gamma_2)\rho \quad (29a)$$

and

$$\omega' \left(t' - \frac{\rho'}{c} \right) = (\Omega_1 + \Omega_2)t - (\Gamma_1 + \Gamma_2)\rho. \quad (29b)$$

By adding or subtracting Eqs. (29a) and (29b), we obtain

$$t' = T(t, \rho) = \frac{t - (\rho/c)\beta \cos \theta}{\gamma(1 - \beta^2 \cos^2 \theta)}, \quad (30a)$$

$$\rho' = R(\rho, t) = \frac{\rho - ct\beta \cos \theta}{\gamma(1 - \beta^2 \cos^2 \theta)}, \quad (30b)$$

and

$$t' \pm \frac{\rho'}{c} = T(t, \rho) \pm \frac{R(\rho, t)}{c} = \frac{t \pm (\rho/c)}{\gamma(1 \pm \beta \cos \theta)}. \quad (30c)$$

Equation (30) shows how lightcone variables in the boost frame are Lorentz transformed into the laboratory frame. Hereafter, the variables T and R will be used as short expressions for representing $T(t, \rho)$ and $R(\rho, t)$.

The Lorentz transformations for the full electric and magnetic fields from the boost frame to the laboratory frame (\mathcal{L}_2) are given by

$$\vec{E}''_{\parallel} = \vec{E}'_{\parallel}, \quad \vec{B}''_{\parallel} = \vec{B}'_{\parallel}, \quad (31a)$$

$$\vec{E}''_{\perp} = \gamma(\vec{E}'_{\perp} - c\vec{\beta} \times \vec{B}'_{\perp}), \quad (31b)$$

and

$$\vec{B}''_{\perp} = \gamma(\vec{B}'_{\perp} + \vec{\beta} \times \vec{E}'_{\perp}/c). \quad (31c)$$

Since the parallel polarization components for the field remain unchanged through the Lorentz transformation, we have

$$\begin{aligned} E''_{f,z',\pm} &= E'_{f,z',\pm} \\ &= -iE'_p(\omega')a_{\pm} \sin \theta'_{\pm} \end{aligned} \quad (32a)$$

and

$$B''_{f,z',\pm} = B'_{f,z',\pm} = 0. \quad (32b)$$

The perpendicular components for the focused fields in the laboratory frame are expressed as

$$\begin{aligned} \begin{bmatrix} E''_{f,x',\pm}(\omega') \\ E''_{f,y',\pm}(\omega') \end{bmatrix} &= \gamma \begin{bmatrix} E'_{f,x',\pm} + c\beta B'_{f,y',\pm} \\ E'_{f,y',\pm} - c\beta B'_{f,x',\pm} \end{bmatrix} \\ &= \gamma E'_p(\omega')(ia_{\pm} \cos \theta_{\pm} + \beta b_{\pm} \sin \theta_{\pm}) \begin{bmatrix} \cos \phi' \\ \sin \phi' \end{bmatrix} \end{aligned} \quad (33a)$$

and

$$\begin{aligned} \begin{bmatrix} B''_{f,x',\pm}(\omega') \\ B''_{f,y',\pm}(\omega') \end{bmatrix} &= \gamma \begin{bmatrix} B'_{f,x',\pm} - (\beta/c)E'_{f,y',\pm} \\ B'_{f,y',\pm} + (\beta/c)E'_{f,x',\pm} \end{bmatrix} \\ &= \frac{\gamma}{c} E'_p(\omega')(b_{\pm} \sin \theta_{\pm} \\ &\quad + i\beta a_{\pm} \cos \theta_{\pm}) \begin{bmatrix} -\sin \phi' \\ \cos \phi' \end{bmatrix}. \end{aligned} \quad (33b)$$

The final field expression can be obtained by summing incoming and outgoing fields as

$$\begin{aligned} \begin{bmatrix} E''_{f,x''}(\omega') \\ E''_{f,y''}(\omega') \end{bmatrix} &= \gamma \begin{bmatrix} E'_{f,x'} + c\beta B'_{f,y'} \\ E'_{f,y'} - c\beta B'_{f,x'} \end{bmatrix} \\ &= \gamma E'_p(\omega')(ia' + \beta b') \begin{bmatrix} \cos \phi' \\ \sin \phi' \end{bmatrix}, \end{aligned} \quad (34a)$$

$$\begin{aligned} \begin{bmatrix} B''_{f,x''}(\omega') \\ B''_{f,y''}(\omega') \end{bmatrix} &= \gamma \begin{bmatrix} B'_{f,x'} - (\beta/c)E'_{f,y'} \\ B'_{f,y'} + (\beta/c)E'_{f,x'} \end{bmatrix} \\ &= \frac{\gamma}{c} E'_p(\omega')(b' + i\beta a') \begin{bmatrix} -\sin \phi' \\ \cos \phi' \end{bmatrix}, \end{aligned} \quad (34b)$$

$$E''_{f,z''}(\omega') = -iE'_p(\omega')(a_{\text{out}} \sin \theta'_{-} + a_{\text{in}} \sin \theta'_{+}), \quad (34c)$$

and

$$B''_{f,z''}(\omega') = 0. \quad (34d)$$

Here, a' and b' in Eq. (34) are expressed as

$$a' = a_{-} \cos \theta'_{-} + a_{+} \cos \theta'_{+} \quad (35a)$$

and

$$b' = b_{-} \sin \theta'_{-} + b_{+} \sin \theta'_{+}, \quad (35b)$$

with a_{\pm} and b_{\pm} defined in Eq. (22). Equation (34) represents the focused electric and magnetic field distributions at a certain angular frequency, but it is still expressed in terms of four-vector components in the boost frame.

D. Spatiotemporal field distribution in the laboratory frame

By using the same analogy as in Eqs. (3) and (8) and taking the Fourier transformation in the ω' space, the spatiotemporal field distribution of the RLF in the laboratory frame is obtained as

$$\vec{E}''_f = \int_{-\infty}^{\infty} d\omega' \vec{E}''_f(\omega') e^{i\omega' t'} = \gamma \begin{bmatrix} (iI_1 + \beta I_2) \cos \phi' \\ (iI_1 + \beta I_2) \sin \phi' \\ -i(1/\gamma)I_3 \end{bmatrix} \quad (36a)$$

and

$$\vec{B}''_f = \int_{-\infty}^{\infty} d\omega' \vec{B}''_f(\omega') e^{i\omega' t'} = \frac{\gamma}{c} \begin{bmatrix} -(I_2 + i\beta I_1) \sin \phi' \\ (I_2 + i\beta I_1) \cos \phi' \\ 0 \end{bmatrix}. \quad (36b)$$

Here, I_n ($n = 1, 2, 3$) are definite integrals defined as

$$\begin{aligned} I_1 &= \int_{-\infty}^{\infty} d\omega' E'_p(\omega') a' e^{i\omega' t'} \\ &= \frac{C_f \sqrt{\mathcal{I}}}{4c} \int_{-\infty}^{\infty} d\omega' \omega' G(\omega') a' e^{i\omega' t'}, \end{aligned} \quad (37a)$$

$$\begin{aligned} I_2 &= \int_{-\infty}^{\infty} d\omega' E'_p(\omega') b' e^{i\omega' t'} \\ &= \frac{C_f \sqrt{\mathcal{I}}}{4c} \int_{-\infty}^{\infty} d\omega' \omega' G(\omega') b' e^{i\omega' t'}, \end{aligned} \quad (37b)$$

and

$$I_3 = \frac{C_f \sqrt{\mathcal{I}}}{4c} \int_{-\infty}^{\infty} d\omega' \omega' G(\omega') (a_{\text{out}} \sin \theta'_- + a_{\text{in}} \sin \theta'_+) e^{i\omega' t'}, \quad (37c)$$

with Eq. (18). These integrals can be calculated with the help of Lorentz transformation given by Eq. (26). For example, the integral I_1 can be first separated into incoming and outgoing parts as

$$\begin{aligned} I_1 &= \frac{C_f \sqrt{\mathcal{I}}}{8i\rho'} \cos \theta'_+ \int_{-\infty}^{\infty} d\omega' e^{i\omega' (t' + \frac{\rho'}{c})} e^{-\frac{(\omega' - \omega'_0)^2}{2\Delta\omega'^2}} \\ &\quad - \frac{C_f \sqrt{\mathcal{I}}}{8i\rho'} \cos \theta'_- \int_{-\infty}^{\infty} d\omega' e^{i\omega' (t' - \frac{\rho'}{c})} e^{-\frac{(\omega' - \omega'_0)^2}{2\Delta\omega'^2}}. \end{aligned} \quad (38)$$

Then, after applying the Lorentz transformation [Eqs. (25) and (30c)] to the coordinates, we obtain

$$\begin{aligned} I_1 &= \frac{C_f \sqrt{\mathcal{I}}}{8i\rho'} \frac{\cos \theta + \beta}{1 + \beta \cos \theta} \int_{-\infty}^{\infty} d\omega' e^{i\frac{\omega' (t + \rho/c)}{\gamma(1 + \beta \cos \theta)}} e^{-\frac{(\omega' - \omega'_0)^2}{2\Delta\omega'^2}} \\ &\quad - \frac{C_f \sqrt{\mathcal{I}}}{8i\rho'} \frac{\cos \theta - \beta}{1 - \beta \cos \theta} \int_{-\infty}^{\infty} d\omega' e^{i\frac{\omega' (t - \rho/c)}{\gamma(1 - \beta \cos \theta)}} e^{-\frac{(\omega' - \omega'_0)^2}{2\Delta\omega'^2}}. \end{aligned} \quad (39)$$

Now, by using the relationship obtained in Eq. (27) and the linear shift of the angular frequency of $\tilde{\omega}_{\pm} = \omega'_{\pm} - \omega'_{0,\pm}$, Eq. (39) is rewritten in the form

$$\begin{aligned} I_1 &= \frac{C_f \sqrt{\mathcal{I}}}{8i\rho'} \gamma (\cos \theta + \beta) e^{i\omega'_{0,+} (t + \frac{\rho}{c})} \\ &\quad \times \int_{-\infty}^{\infty} d\tilde{\omega}_+ \exp \left[i\tilde{\omega}_+ \left(t + \frac{\rho}{c} \right) \right] \exp \left[-\frac{\tilde{\omega}_+^2}{\Delta\omega'^2_+} \right] \\ &\quad - \frac{C_f \sqrt{\mathcal{I}}}{8i\rho'} \gamma (\cos \theta - \beta) e^{i\omega'_{0,-} (t - \frac{\rho}{c})} \\ &\quad \times \int_{-\infty}^{\infty} d\tilde{\omega}_- \exp \left[i\tilde{\omega}_- \left(t - \frac{\rho}{c} \right) \right] \exp \left[-\frac{\tilde{\omega}_-^2}{\Delta\omega'^2_-} \right]. \end{aligned} \quad (40)$$

Again, the center frequency and the spectral bandwidth, $\omega'_{0,\pm}$ and $\Delta\omega'_{\pm}$, in the laboratory frame (\mathcal{L}_2) are defined as

$$\omega'_{0,\pm} = \frac{\omega'_0}{\gamma(1 \pm \beta \cos \theta)} \quad \text{and} \quad \Delta\omega'_{\pm} = \frac{\Delta\omega'_0}{\gamma(1 \pm \beta \cos \theta)}, \quad (41)$$

by Eq. (27). Using the integral identity [56] of

$$\begin{aligned} &\int_0^{\infty} x^{p-1} e^{-qx^2} \cos sx dx \\ &= \frac{1}{2} q^{-p/2} \Gamma\left(\frac{p}{2}\right) \exp\left(-\frac{s^2}{4q}\right) {}_1F_1\left(-\frac{p}{2} + \frac{1}{2}; \frac{1}{2}; \frac{s^2}{4q}\right), \end{aligned} \quad (42)$$

the integral

$$\int_{-\infty}^{\infty} d\tilde{\omega}_{\pm} \cos \tilde{\omega}_{\pm} \left(t \pm \frac{\rho}{c} \right) e^{-\tilde{\omega}_{\pm}^2 / \Delta\omega'^2_{\pm}} \quad (43)$$

becomes

$$\sqrt{\pi} \Delta\omega'^2_{\pm} \exp \left[-\frac{\Delta\omega'^2_{\pm} (t \pm \rho/c)^2}{4} \right], \quad (44)$$

with $p = 1$, $q = 1/\Delta\omega'^2_{\pm}$, and $s = t \pm \rho/c$, since $\Gamma(1/2) = \sqrt{\pi}$ and ${}_1F_1(0; 1/2; s^2/4q) = 1$. Here, $\Gamma(\cdot)$ and ${}_1F_1(\cdot)$ are the Gamma function and the confluent hypergeometric function. Note that $\int_{-\infty}^{\infty} e^{-qx^2} \sin sx dx = 0$. Finally, after integrating over $(-\infty, \infty)$, Eq. (40) becomes

$$\begin{aligned} I_1 &= \sqrt{\pi} \frac{\Delta\omega' C_f}{8iR} \sqrt{\mathcal{I}} \frac{\cos \theta + \beta}{1 + \beta \cos \theta} e^{i\omega'_0 (T+R/c)} \\ &\quad \times \exp \left[-\frac{\Delta\omega'^2}{4} \left(T + \frac{R}{c} \right)^2 \right] \\ &\quad - \sqrt{\pi} \frac{\Delta\omega' C_f}{8iR} \sqrt{\mathcal{I}} \frac{\cos \theta - \beta}{1 - \beta \cos \theta} e^{i\omega'_0 (T-R/c)} \\ &\quad \times \exp \left[-\frac{\Delta\omega'^2}{4} \left(T - \frac{R}{c} \right)^2 \right], \end{aligned} \quad (45)$$

with the help of Eq. (30). This integral contains information on the incoming ($T + R/c$) and outgoing ($T - R/c$) spherical fields in the $R - T$ space. These incoming and outgoing fields can be expressed with spherical Bessel functions as

$$\frac{e^{i\omega'_0 (T \pm R/c)}}{R} = \frac{\omega'_0}{c} \left[y_0 \left(\frac{\omega'_0}{c} R \right) \pm j_0 \left(\frac{\omega'_0}{c} R \right) \right] e^{i\omega'_0 T}, \quad (46)$$

where $j_0(\cdot)$ and $y_0(\cdot)$ are the spherical Bessel functions of the first and the second kinds, respectively. Since the functional value of $y_0(\omega'_0 R/c)$ is infinity at $R = 0$, we take the imaginary part from Eq. (46) as the solution of Eq. (45). Then, we have

$$I_1 = \frac{\sqrt{\pi} \omega'_0 \Delta\omega' C_f \sqrt{\mathcal{I}}}{4c} j_0 \left(\frac{\omega'_0}{c} R \right) \Upsilon_1 e^{i\omega'_0 T}, \quad (47)$$

with the definition of the envelope function of

$$\begin{aligned} \Upsilon_1 &= \frac{1}{2} \left\{ \frac{\cos \theta + \beta}{1 + \beta \cos \theta} \exp \left[-\frac{\Delta\omega'^2}{4} \left(T + \frac{R}{c} \right)^2 \right] \right. \\ &\quad \left. + \frac{\cos \theta - \beta}{1 - \beta \cos \theta} \exp \left[-\frac{\Delta\omega'^2}{4} \left(T - \frac{R}{c} \right)^2 \right] \right\}. \end{aligned} \quad (48)$$

Similarly, by applying the same mathematical procedures, we obtain the following results for the other integrals:

$$I_2 = \frac{\sqrt{\pi} \omega'_0 \Delta\omega' C_f \sqrt{\mathcal{I}}}{4c} j_1 \left(\frac{\omega'_0}{c} R \right) \Upsilon_2 e^{i\omega'_0 T} \quad (49a)$$

and

$$I_3 = \frac{\sqrt{\pi}\omega'_0\Delta\omega' C_f\sqrt{\mathcal{I}}}{4c} j_0\left(\frac{\omega'_0}{c}R\right)\Upsilon_2 e^{i\omega'_0 T}, \quad (49b)$$

with the definition of another envelope function,

$$\Upsilon_2 = \frac{1}{2} \left\{ \frac{\sin\theta}{\gamma(1-\beta\cos\theta)} \exp\left[-\frac{\Delta\omega'^2}{4}\left(T-\frac{R}{c}\right)^2\right] + \frac{\sin\theta}{\gamma(1+\beta\cos\theta)} \exp\left[-\frac{\Delta\omega'^2}{4}\left(T+\frac{R}{c}\right)^2\right] \right\}. \quad (50)$$

Now, inserting Eqs. (47) and (49) into Eq. (36), the general mathematical expressions for the spatiotemporal field distribution of the RLF with the radial polarization are obtained as

$$\begin{aligned} \vec{E}_f'' &= \gamma \frac{\sqrt{\pi}\omega'_0\Delta\omega' C_f\sqrt{\mathcal{I}}}{4c} \\ &\times \begin{bmatrix} \{-j_0 \sin(\omega'_0 T)\Upsilon_1 + \beta j_1 \cos(\omega'_0 T)\Upsilon_2\} \cos\phi \\ \{-j_0 \sin(\omega'_0 T)\Upsilon_1 + \beta j_1 \cos(\omega'_0 T)\Upsilon_2\} \sin\phi \\ (1/\gamma)j_0 \sin(\omega'_0 T)\Upsilon_2 \end{bmatrix} \end{aligned} \quad (51a)$$

and

$$\begin{aligned} \vec{B}_f'' &= \frac{\gamma}{c} \frac{\sqrt{\pi}\omega'_0\Delta\omega' C_f\sqrt{\mathcal{I}}}{4c} \\ &\times \begin{bmatrix} \{-j_1 \cos(\omega'_0 T)\Upsilon_2 - \beta j_0 \sin(\omega'_0 T)\Upsilon_1\} \sin\phi \\ \{j_1 \cos(\omega'_0 T)\Upsilon_2 - \beta j_0 \sin(\omega'_0 T)\Upsilon_1\} \cos\phi \\ 0 \end{bmatrix} \end{aligned} \quad (51b)$$

in the laboratory frame. In Eq. (51), the azimuthal angle ϕ' is replaced by ϕ due to $\phi' = \phi$, and $j_{0,1}$ should read $j_{0,1}(\omega'R/c)$. Equation (51) is valid in the relativistic limit since the 4π -spherical focusing scheme that is used is valid only when $\gamma \gg 1$.

When the TE mode (azimuthally polarized) laser pulse is incident and focused by the RFFPM, from the symmetry in the polarization, the EM field distributions of the 4π -spherically focused monochromatic TE mode EM wave are expressed as

$$\begin{aligned} \vec{E}'_f(x'^{\mu}; \omega') &= -\hat{\phi}' E'_p(\omega') b(\rho', \theta'; \omega') e^{i\omega' t'} \\ &= \vec{E}'_{f,\parallel} \end{aligned} \quad (52a)$$

and

$$\begin{aligned} \vec{B}'_f(x'^{\mu}; \omega') &= \hat{\theta}' i B'_p(\omega') a(\rho', \theta'; \omega') e^{i\omega' t'} \\ &= \vec{B}'_{f,\perp} + \vec{B}'_{f,\parallel}. \end{aligned} \quad (52b)$$

In this case, followed by the similar mathematical procedures taken as before, the general mathematical expressions for the spatiotemporal field distribution of the RLF with the azimuthal polarization are obtained as

$$\begin{aligned} \vec{E}_f'' &= \gamma \frac{\sqrt{\pi}\omega'_0\Delta\omega' C_f\sqrt{\mathcal{I}}}{4c} \\ &\times \begin{bmatrix} \{-j_1 \cos(\omega'_0 T)\Upsilon_2 - \beta j_0 \sin(\omega'_0 T)\Upsilon_1\} \sin\phi \\ \{j_1 \cos(\omega'_0 T)\Upsilon_2 - \beta j_0 \sin(\omega'_0 T)\Upsilon_1\} \cos\phi \\ 0 \end{bmatrix} \end{aligned} \quad (53a)$$

and

$$\begin{aligned} \vec{B}_f'' &= \frac{\gamma}{c} \frac{\sqrt{\pi}\omega'_0\Delta\omega' C_f\sqrt{\mathcal{I}}}{4c} \\ &\times \begin{bmatrix} \{-j_0 \sin(\omega'_0 T)\Upsilon_1 + \beta j_1 \cos(\omega'_0 T)\Upsilon_2\} \cos\phi \\ \{-j_0 \sin(\omega'_0 T)\Upsilon_1 + \beta j_1 \cos(\omega'_0 T)\Upsilon_2\} \sin\phi \\ (1/\gamma)j_0 \sin(\omega'_0 T)\Upsilon_2 \end{bmatrix}. \end{aligned} \quad (53b)$$

In Eqs. (51) and (53), the peak field strength of the E-field of RLF can be rewritten as

$$\begin{aligned} \gamma \frac{\sqrt{\pi}\omega'_0\Delta\omega' C_f\sqrt{\mathcal{I}}}{4c} &= \gamma \frac{1+\beta}{1-\beta} \frac{\sqrt{\pi}\omega_0\Delta\omega C_f\sqrt{\mathcal{I}}}{4c} \\ &= \gamma \frac{1+\beta}{1-\beta} \sqrt{\frac{3\pi}{c\epsilon_0}} \frac{\pi\omega_0 w_e \sqrt{\mathcal{I}_p}}{4c}, \end{aligned} \quad (54)$$

with the definition of the intensity, $\mathcal{I}_p (= \Delta\omega^2 \mathcal{I})$, in time shown in Sec. II. So, it is clear that in the relativistic limit of $\beta \rightarrow 1$, the field strength and the intensity are enhanced by a factor of $\gamma^3 (w_e/\lambda_0)$ and $\gamma^6 (w_e/\lambda_0)^2$, as discovered in [43]. Comparing the intensity enhancement given by the RFFM case, the RFFM gives an additional enhancement of a factor of $(3\pi^5/8)\gamma^2 (w_e/\lambda_0)^2$ with an incident beam size of $D = 2w_e$.

The change in the angular frequency of the RLF can be calculated by decomposing the spherical Bessel function into the incoming and outgoing fields again. The phase for the incoming or outgoing field is given by $\omega'_0 T \pm \omega'_0 R/c$ or $[(1+\beta)/(1\pm\beta\cos\theta)]\omega_0(t \pm \rho/c)$ in Eqs. (51) and (53). Thus, the angular frequency for the outgoing laser pulse is enhanced by $(1+\beta)/(1-\beta)$ in the forward direction ($\theta = 0$) or $\sim 4\gamma^2$ in the relativistic limit, which is consistent with the result from the RFFM case. The change in the nominal pulse duration of the outgoing laser pulse is determined by the argument of $\Delta\omega'^2 (T - R/c)^2/4$ in Eq. (48) or (50). From the argument, it is clear that the nominal pulse duration τ_F'' of the RLF in the laboratory frame is given by $(1/\Delta\omega)(1-\beta\cos\theta)/(1+\beta)$. In the forward direction ($\theta = 0$), the nominal pulse duration is reduced by a factor of $(1-\beta)/(1+\beta)$, which is also consistent with the RFFM case. Although Eqs. (51) and (53) well describe the field distribution and its propagation of the RLF, its limitation should be addressed here. In this study, an ideal RFFM, which has a constant velocity and a flat perfect reflectance over the wavelength and incidence angle, is assumed and the recoil effect happening during the reflection of the incident strong laser pulse [57] is ignored. Therefore, obtaining a mathematical expression for the RLF under a more realistic circumstance will be the next step to be pursued.

Figure 3 shows the squared electric field ($E^2 = E_x^2 + E_z^2$) distribution of the RLF at different times. The center frequency (ω_0) of the incident laser pulse is $\sim 2.36 \times 10^{15}$ rad/s, assuming the center wavelength of $0.8 \mu\text{m}$. The Gaussian width ($\Delta\omega$) of the spectrum is 1.77×10^{14} rad/s, supporting a FWHM pulse duration of ~ 9.4 fs. The first row in Fig. 3 presents the squared electric field at $\gamma = 1$. The electric and magnetic fields are separated in space and time, and the field oscillates with a period ($\mathcal{T}_{\text{period}} = 2\pi/\omega_0$) of ~ 2.67 fs. The second row presents the squared electric field at $\gamma = 10$. In this case, the squared field is expressed in the logarithmic scale, and it is normalized by the peak laser intensity of the

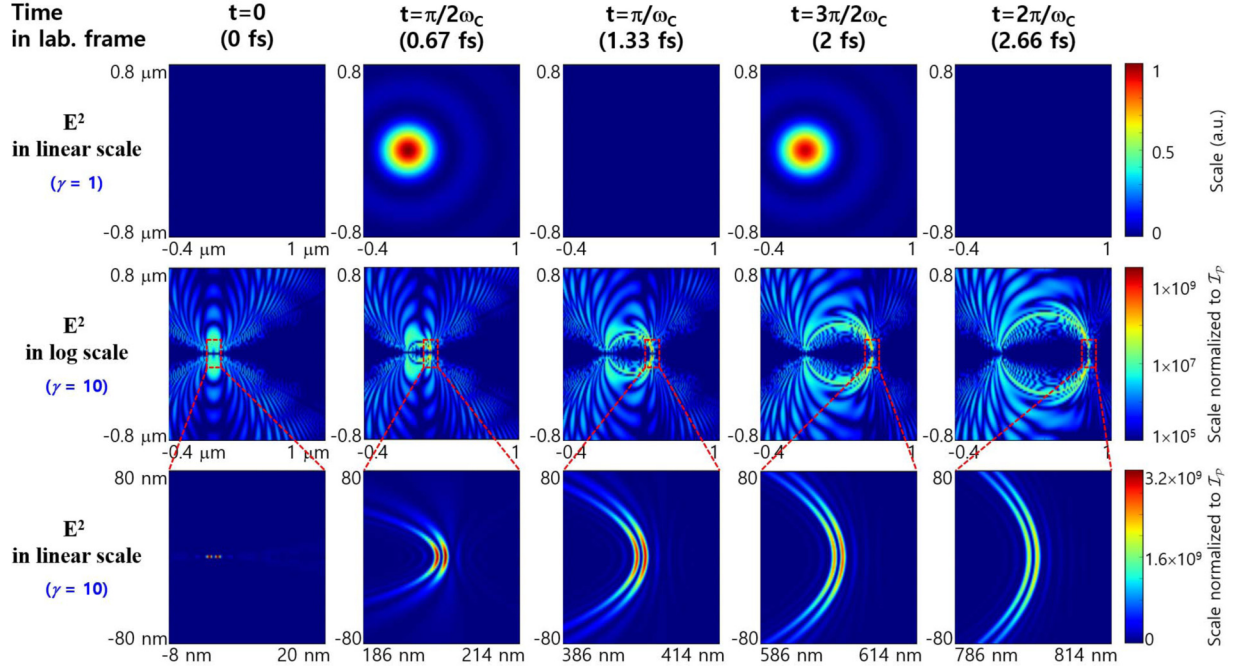


FIG. 3. The squared electric field distribution calculated from Eq. (51). The squared electric field distribution is expressed in the x - z (vertical-horizontal) plane. In this plane, $E''_{f,y}$ becomes zero since $\phi = 0$. The electric field distributions in the first row are calculated under $\gamma = 1$, i.e., the mirror is stationary. The field distribution agrees well with the characteristics obtained under the 4π -spherical focusing condition. The squared electric field distributions in the second and third rows are calculated under $\gamma = 10$. The field distribution travels with a relativistic velocity of $c\beta = c\sqrt{(\gamma^2 - 1)}/\gamma^2$ as shown in the third row, and the peak field strength is enhanced by a factor given by Eq. (54).

RLF given by the square of Eq. (54). The third row presents an enlarged view of the red dashed area in the second row. The spot size of the peak calculated from the second-order moment is ~ 2.5 nm, which is close to the nominal wavelength of 2.0 nm obtained from $\lambda_0/4\gamma^2$. The second and third rows clearly show that the RLF travels at a relativistic speed of βc and how its field distribution propagates in time over several hundreds of nm in range.

E. Recoil effect with a low mirror reflection

The field calculation, so far, has been based on an ideal mirror which has perfect reflectance, i.e., $\mathcal{R} = 1$. However, the reflectance of the mirror is dependent on the mirror model and is, in general, very low [46,53,58,59]. Due to a low mirror reflectance, most of the incident (source) pulse energy is transmitted through the mirror, which leads to much lower distortion in the flying mirror than expected. The low reflection of the mirror minimizes the change in mirror shape during reflection. Here we explain how the low mirror reflectance reduces the recoil effect on the frequency upshift, and show that the beam radius-wavelength ratio can further intensify the focused intensity toward the nonlinear QED regime even with a low reflectance of the mirror.

From momentum and energy conservation, we rewrite Eqs. (3) and (4) of [57] in two-dimensional form as

$$n_e p_e - n_\omega p_\omega = n_e p'_e \cos \theta_e + \mathcal{R} n_\omega p''_\omega \cos \theta - (1 - \mathcal{R}) n_\omega p_\omega, \quad (55a)$$

$$0 = n_e p'_e \sin \theta_e - \mathcal{R} n_\omega p''_\omega \sin \theta, \quad (55b)$$

where θ_e and θ refer to the angles for the electron and photon after reflection, respectively, and

$$n_e \varepsilon_e + n_\omega \varepsilon_\omega = n_e \varepsilon'_e + \mathcal{R} n_\omega \varepsilon''_\omega + (1 - \mathcal{R}) n_\omega \varepsilon_\omega. \quad (55c)$$

Here, p and ε refer to the momentum and energy for the individual electron and photon, and the subscripts e and ω are used to denote the electron and photon. n_e and n_ω are population densities for the electron and photon. The reflectance \mathcal{R} depends on the incident angle, but, considering the mathematical simplicity and aperture function, we ignore the angle dependency for the mirror. The unprimed and double-primed quantities refer to quantities before and after reflection. Equations (55a) and (55b) can be combined by use of $\sin^2 \theta_e + \cos^2 \theta_e = 1$ to yield

$$n_e^2 p_e'^2 = n_e^2 p_e^2 + \mathcal{R}^2 n_\omega^2 p_\omega'^2 + \mathcal{R}^2 n_\omega^2 p_\omega^2 - 2\mathcal{R} n_e n_\omega p_e p_\omega' \cos \theta - 2\mathcal{R} n_e n_\omega p_e p_\omega + 2\mathcal{R}^2 n_\omega^2 p_\omega p_\omega' \cos \theta, \quad (56)$$

and, subtracting $n_e^2 p_e'^2 c^2$ from $n_e^2 \varepsilon_e'^2$, we obtain

$$n_e^2 (\varepsilon_e'^2 - p_e'^2 c^2) = n_e^2 (\varepsilon_e^2 - p_e^2 c^2) + \mathcal{R}^2 n_\omega^2 (\varepsilon_\omega^2 - p_\omega^2 c^2) + \mathcal{R}^2 n_\omega^2 (\varepsilon_\omega'^2 - p_\omega'^2 c^2) + 2\mathcal{R} n_\omega n_e (\varepsilon_e \varepsilon_\omega + p_e p_\omega c^2) - 2\mathcal{R} n_\omega n_e (\varepsilon_e \varepsilon_\omega' - p_e p_\omega' c^2 \cos \theta) - 2\mathcal{R}^2 n_\omega^2 (\varepsilon_\omega \varepsilon_\omega' + p_\omega p_\omega' c^2 \cos \theta). \quad (57)$$

Since $\varepsilon_e''^2 - p_e''^2 c^2 = \varepsilon_e^2 - p_e^2 c^2 = m_e^2 c^4$ for electrons and $\varepsilon_\omega''^2 - p_\omega''^2 c^2 = \varepsilon_\omega^2 - p_\omega^2 c^2 = 0$ for photons, Eq. (57) becomes

$$[n_e(\varepsilon_e - p_e c \cos \theta) + \mathcal{R} n_\omega \varepsilon_\omega (1 + \cos \theta)] \frac{\varepsilon_\omega''}{\varepsilon_\omega} = n_e(\varepsilon_e + p_e c). \quad (58)$$

Here, m_e is the electron mass. Then, with the help of $p_e c = \beta \varepsilon_e$, we obtain

$$\varepsilon_\omega'' = \varepsilon_\omega \frac{n_e \varepsilon_e (1 + \beta)}{n_e \varepsilon_e (1 - \beta \cos \theta) + \mathcal{R} n_\omega \varepsilon_\omega (1 + \cos \theta)}. \quad (59)$$

The energy density can be further expressed as

$$n_e \varepsilon_e = \gamma n_e m_e c^2 \quad \text{and} \quad n_\omega \varepsilon_\omega = \mathcal{I}/c. \quad (60)$$

The ratio $\mathcal{R} n_\omega \varepsilon_\omega / n_e \varepsilon_e = \mathcal{R} \mathcal{I} / \gamma n_e m_e c^3$ in Eq. (59) can be expressed as $\sim 3 \times 10^{19} \times (\mathcal{R}/n_e)$ at $\mathcal{I} = 2.3 \times 10^{17}$ W/cm² in terms of the reflectance and the electron density of the mirror. The reflectance \mathcal{R} is very low. For example, according to the thin foil electron layer mirror model, the reflectance of the mirror is given by $\mathcal{R} = 0.5\gamma^{-3}$ [53,58,59] and yields 2.75×10^{-4} for a Lorentz γ of 12.2. Thus, the frequency for reflected photons can be approximated as

$$\omega'' \approx \omega \frac{1 + \beta}{1 - \beta \cos \theta} \times \left[1 - \frac{\mathcal{R} \mathcal{I}_0}{\gamma n_e m_e c^3} (1 + \cos \theta)^2 e^{-\frac{\sin^2 \theta}{\sin^2 \theta_0}} \right]. \quad (61)$$

Here, the laser intensity \mathcal{I} is replaced by $\mathcal{I}_0 \sin^2 \theta e^{-\sin^2 \theta / \sin^2 \theta_0}$, which is the incident intensity distribution for the TM or TE mode beam profile. Comparing Eq. (61) to the well-known frequency upshift formula $\omega'' = \omega(1 + \beta)/(1 - \beta \cos \theta)$, the second term in the bracket on the right-hand side gives the correction to the wavelength shift by the recoil effect. Equation (61) shows how the frequency upshift for the curved mirror is modified by the recoil effect when the mirror reflectance is considered. Since $\mathcal{R} \mathcal{I}_0 / \gamma n_e m_e c^3 \ll 1$ at a source laser power of 180 TW or an intensity \mathcal{I}_0 of 2.3×10^{17} W/cm², the frequency shift is approximated as $\omega'' \approx \omega(1 + \beta)/(1 - \beta \cos \theta)$. In addition, the consideration of a low reflectance of \mathcal{R} does not allow violation of the energy balance condition through $n_\omega'' \hbar \omega'' \approx \mathcal{R}(4\gamma^2 \mathcal{I}_0/c) < \gamma n_e m_e c^2$. A numerical calculation shows that energy densities [$\mathcal{R}(4\gamma^2 \mathcal{I}_0/c)$ and $\gamma n_e m_e c^2$] for the reflected laser pulse and the electron layer acting as the RFM are $\sim 1.25 \times 10^6$ J/cm³ and $\sim 1 \times 10^7$ J/cm³ with a γ -factor of 12.2, respectively. So, it is valid to apply the approach used in previous sections when calculating the field distribution since it does not seriously modify the frequency upshift and the field distribution with a low reflectance. However, the low reflectance affects the reflected energy, and consequently the peak intensity of a focused laser field and the e^+e^- pair production rate, as discussed in the following section.

After reflection, the frequency-upshifted source laser pulse is further intensified by the beam radius-wavelength ratio w_e/λ_0 , as shown in Eqs. (53) and (54). This factor first appeared in the original paper on the RFM [46] and results in the intensification of the electromagnetic pulse, while maintaining a substantially low source laser intensity on the mirror

with a substantially large beam size. With a given reflectance of \mathcal{R} , the peak electric field strength of a focused field can be written from Eqs. (53a) and (54) as

$$E_f'' = \sqrt{\mathcal{R}} \gamma \frac{1 + \beta}{1 - \beta} \sqrt{\frac{3\pi}{c\varepsilon_0} \frac{\pi \omega w_e}{4c}} \sqrt{\mathcal{I}}. \quad (62)$$

Under the condition of $E_f'' = E_{\text{Sch}}$, Eq. (62) can be reexpressed as

$$\mathcal{I} = \frac{(\lambda_0/w_e)^2}{6\pi^5 R \gamma^6} \mathcal{I}_{\text{Sch}}, \quad (63)$$

with the definition of $\mathcal{I}_{\text{Sch}} = (1/2)c\varepsilon_0 E_{\text{Sch}}^2 \approx 2.3 \times 10^{29}$ W/cm². Then, the source laser intensity \mathcal{I} required for reaching the Schwinger field is calculated to be $\sim 2.27 \times 10^{17}$ W/cm² with parameters such as $\gamma = 12.2$, $\lambda = 0.2 \mu\text{m}$, $w_0 = 156 \mu\text{m}$, and $\mathcal{R} = 0.1\gamma^{-3}$. Thus, the beam radius-wavelength ratio plays a critical role in boosting the focused field strength to the nonlinear QED regime.

IV. PAIR PRODUCTION UNDER THE RLF FIELD

Until now, the analytical field expression for the TM or TE mode RLF has been obtained in the laboratory frame. In this section, the electron-positron (e^+e^-) pair production rate is investigated with the field expressions obtained in the relativistic limit. Here we consider the Schwinger mechanism for the pair production.

A. Invariant fields and pair production rate

Assuming the Compton wavelength is much less than the wavelength of the RLF [19,60–62], the spacetime-dependent e^+e^- pair production rate W_{ep} can be calculated from

$$W_{ep} = \frac{e^2 E_{\text{Sch}}^2}{4\pi^3 \hbar^2 c} E_{\text{inv}} B_{\text{inv}} \coth \left(\pi \frac{B_{\text{inv}}}{E_{\text{inv}}} \right) e^{-\pi/E_{\text{inv}}}. \quad (64)$$

Here, E_{inv} and B_{inv} are invariant fields defined by

$$E_{\text{inv}} = \frac{\sqrt{(\mathcal{F}^2 + \mathcal{G}^2)^{1/2} - \mathcal{F}}}{E_{\text{Sch}}} \quad (65a)$$

and

$$B_{\text{inv}} = \frac{\sqrt{(\mathcal{F}^2 + \mathcal{G}^2)^{1/2} + \mathcal{F}}}{E_{\text{Sch}}}. \quad (65b)$$

In Eq. (65), the Poincaré invariants \mathcal{F} and \mathcal{G} for the RLF are calculated as

$$\mathcal{F} = \frac{c^2 B^2 - E^2}{2} \quad \text{and} \quad \mathcal{G} = c \vec{B} \cdot \vec{E}. \quad (66)$$

Then, the Poincaré invariants for the TM mode laser pulse can be calculated with Eq. (51) and become

$$\begin{aligned} \mathcal{F}_{\text{TM}} &= \frac{1}{2} \left(\frac{1 + \beta}{1 - \beta} \frac{\sqrt{\pi} \omega_0 C_f \sqrt{\mathcal{I}_p}}{4c} \right)^2 \\ &\quad \times [j_1^2 \cos^2(\omega'_0 T) \Upsilon_2^2 - j_0^2 \sin^2(\omega'_0 T) (\Upsilon_1^2 + \Upsilon_2^2)] \\ &= \frac{1}{2} \left(\frac{1 + \beta}{1 - \beta} \frac{\sqrt{\pi} \omega_0 C_f \sqrt{\mathcal{I}_p}}{4c} \right)^2 j_{\{1-0\}}^2 \end{aligned} \quad (67a)$$

and

$$\mathcal{G}_{\text{TM}} = 0, \quad (67b)$$

where the function $j_{\{1-0\}}^2$ is defined as $j_1^2 \cos^2(\omega'_0 T) \Upsilon_2^2 - j_0^2 \sin^2(\omega'_0 T) (\Upsilon_1^2 + \Upsilon_2^2)$, and j_i represents the spherical Bessel function $j_i(\omega'_0 \rho'/c)$. The invariant fields E_{inv} and H_{inv} are determined by the sign of \mathcal{F} . When $\mathcal{F} \geq 0$ [i.e., $j_1^2 \cos^2(\omega'_0 T) \Upsilon_2^2 \geq j_0^2 \sin^2(\omega'_0 T) (\Upsilon_1^2 + \Upsilon_2^2)$], $\sqrt{\mathcal{F}^2} = \mathcal{F}$. On the other hand, when $\mathcal{F} < 0$, $\sqrt{\mathcal{F}^2} = -\mathcal{F}$. This results in

$$E_{\text{inv}} = \frac{1 + \beta}{1 - \beta} \frac{\sqrt{\pi} \omega_0 C_f \sqrt{\mathcal{I}_p}}{4c E_{\text{Sch}}} \begin{cases} 0, & \mathcal{F} \geq 0 \\ \sqrt{-j_{\{1-0\}}^2}, & \mathcal{F} < 0 \end{cases} \quad (68a)$$

and

$$B_{\text{inv}} = \frac{1 + \beta}{1 - \beta} \frac{\sqrt{\pi} \omega_0 C_f \sqrt{\mathcal{I}_p}}{4c^2 E_{\text{Sch}}} \begin{cases} \sqrt{j_{\{1-0\}}^2}, & \mathcal{F} \geq 0 \\ 0, & \mathcal{F} < 0. \end{cases} \quad (68b)$$

Thus, from Eq. (64), it follows that no pair production is expected even with the enhanced field strength of the RLF when $\mathcal{F} \geq 0$. In the other case ($\mathcal{F} < 0$), the e^+e^- pair production rate via the Schwinger mechanism can be explicitly calculated in terms of the Lorentz γ -factor, the beam radius-wavelength ratio (w_e/λ_0), and the laser intensity (\mathcal{I}_p) as

$$W_{ep} \approx 12\pi^2 \alpha \gamma^4 \left(\frac{w_e}{\lambda_0}\right)^2 \left(\frac{\mathcal{I}_p}{\hbar c}\right) (-j_{\{1-0\}}^2) \times \exp \left[-\frac{1}{\gamma^2} \frac{\lambda_0}{w_e} \frac{(E_{\text{Sch}}/E_p)}{\sqrt{6\pi^3} \sqrt{-j_{\{1-0\}}^2}} \right], \quad (69)$$

in the relativistic limit. Here, α is the fine structure constant defined as $e^2/4\pi\hbar c\epsilon_0$ and the peak field strength E_p in time as $\sqrt{2\mathcal{I}_p/c\epsilon_0}$. The e^+e^- pair production occurs only in the region of $j_{\{1-0\}}^2 < 0$.

For the TE mode laser pulse, the e^+e^- pair production rate can be calculated with Eq. (53) and the final form is given by

$$W_{ep} \approx 12\pi^2 \alpha \gamma^4 \left(\frac{w_e}{\lambda_0}\right)^2 \left(\frac{\mathcal{I}_p}{\hbar c}\right) (-j_{\{0-1\}}^2) \times \exp \left[-\frac{1}{\gamma^2} \frac{\lambda_0}{w_e} \frac{(E_{\text{Sch}}/E_p)}{\sqrt{6\pi^3} \sqrt{-j_{\{0-1\}}^2}} \right], \quad (70)$$

where $j_{\{0-1\}}^2$ is defined as $j_0^2 \sin^2(\omega'_0 T) (\Upsilon_1^2 + \Upsilon_2^2) - j_1^2 \cos^2(\omega'_0 T) \Upsilon_2^2$. Again, the e^+e^- pair production occurs only in the region of $j_{\{0-1\}}^2 < 0$.

Now, let us consider the reflectance \mathcal{R} of the flying plasma mirror in the calculation of e^+e^- pair production. The reflectance can be modeled as $0.5\gamma^{-3}$ for the infinitely thin foil model, $\sim 0.1\gamma^{-4}$, for the wake wave model, and a rather complicated form can be found for the double-sided mirror model [53,58,59]. By multiplying the reflectance \mathcal{R} into the

intensity \mathcal{I}_p , the pair production rate can be modified as

$$W_{ep} \approx 6\pi^2 \alpha \gamma \left(\frac{w_e}{\lambda_0}\right)^2 \left(\frac{\mathcal{I}_p}{\hbar c}\right) (-j_{\{0-1\}}^2) \times \exp \left[-\frac{1}{\sqrt{\gamma}} \frac{\lambda_0}{w_e} \frac{(E_{\text{Sch}}/E_p)}{\sqrt{3\pi^3} \sqrt{-j_{\{0-1\}}^2}} \right] \quad (71a)$$

for the thin foil model or

$$W_{ep} \approx 1.2\pi^2 \alpha \left(\frac{w_e}{\lambda_0}\right)^2 \left(\frac{\mathcal{I}_p}{\hbar c}\right) (-j_{\{0-1\}}^2) \times \exp \left[-\frac{\lambda_0}{w_e} \frac{(E_{\text{Sch}}/E_p)}{0.32\sqrt{6\pi^3} \sqrt{-j_{\{0-1\}}^2}} \right] \quad (71b)$$

for the wake wave model. From Eq. (71b), it is obvious that in the case of the wake wave model, due to the reflectance of the mirror, the pair production rate becomes dependent only on the beam radius-wavelength ratio (w_e/λ_0). Thus, the e^+e^- pair production from the thin foil model will be mostly considered.

The total number $N_{e^+e^-}$ of e^+e^- pairs produced by the RLFs can be estimated by integrating the pair production rate W_{ep} over a four-volume [61]. The threshold of the incident

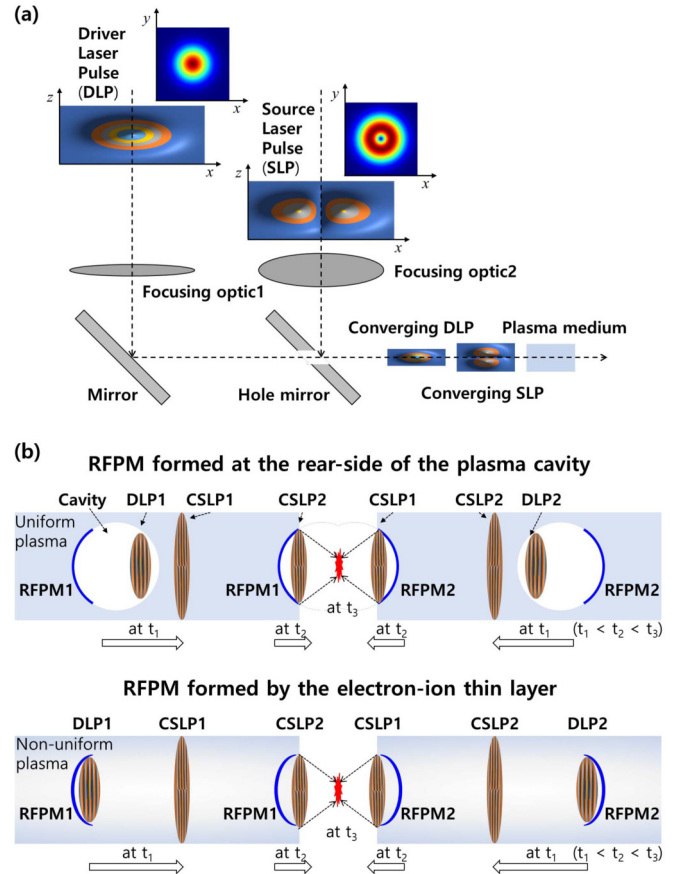


FIG. 4. (a) Schematic diagram for collinear coupling of driver and source laser pulses. (b) Formation of RFPMs and collision in vacuum of two source pulses reflected from the respective RFPMs. CSLP: Converging source laser pulse.

laser power required for a single e^+e^- pair production is examined with a γ -factor of 12.2. Such a relativistic mirror can be driven by focusing a 100 PW Ti:sapphire ($\lambda_0=0.8\ \mu\text{m}$) laser pulse within a focal spot radius of $100\ \mu\text{m}$, assuming the γ -factor of the mirror is given by $\sqrt{1+a_0^2}$. A laser pulse with $a_0=0.1$ and a beam radius w_0 of $100\ \mu\text{m}$ is considered as an incident laser pulse to be reflected. According to [57], in order to minimize the recoil effect, an incident pulse duration should be less than a characteristic time τ_c , given as

$$\tau_c = \kappa \frac{2^{4/3} m_e c^2}{2\Gamma^2(2/3)} \left(\frac{\omega_0}{\omega_{pe}} \right)^{8/3} \gamma_L^{1/3} \frac{n_e \lambda_L}{\mathcal{I}_p}. \quad (72)$$

Here, ω_{pe} is the Langmuir frequency, γ_L the Lorentz γ -factor for the Langmuir wave, and λ_L the Langmuir wavelength. The parameter κ can be obtained from the simulation. Although this analysis is based on a one-dimensional particle-in-cell (PIC) approach, it provides a rough estimation of the maximum pulse duration required for minimizing the recoil effect in time. The calculation with $\kappa = 1.5 \times 10^{-4}$ and an electron density of $0.01 n_{cr}$ shows that the incident laser pulse with an a_0 of 0.1 can have a maximum pulse duration of about 30 fs before the mirror is severely affected by the recoil effect. This pulse duration can be supported by a spectral bandwidth $\Delta\omega$ of 19 nm (~ 32 nm at FWHM). This means that a laser pulse with a pulse duration of ~ 9.4 fs (supported by a spectral bandwidth $\Delta\omega$ of 60 nm at 800 nm center wavelength ω_0) can be used as the incident laser pulse to be reflected. In this case, the minimum reflectance of the mirror required for a single e^+e^- pair production is estimated as $\sim 14.1\%$. The e^+e^- pairs production is strongly suppressed by the low reflectance

($2.7 \times 10^{-2}\%$ for $0.5\gamma^{-3}$ and $4.5 \times 10^{-4}\%$ for $0.1\gamma^{-4}$) of the mirror. The required laser field strengths, expressed as a_0 , increase to ~ 2.8 for the thin foil and ~ 21.6 for the wake wave cases. Under these field strengths, the characteristic time given by Eq. (72) becomes as short as 0.05 fs for the thin foil and 8×10^{-4} fs for the wake wave cases, so the RFPM is destroyed before reaching a field strength required for the single e^+e^- pair production event.

B. Pair production with two counterpropagating RLFs

It is now interesting to consider when two counterpropagating RLFs collide with each other. The experimental setup considered is visualized in Fig. 4. The two (driver and source) laser pulses are coupled by a hole mirror and propagate in a plasma medium. The source laser pulse (SLP1) proceeds ahead to be reflected by the other counterpropagating RFPM formed by another driver laser pulse (DLP2). Two sets of plasma media are prepared to ensure the collision of the reflected SLPs in vacuum. An ideally sharp edge is preferred. Figure 4(b) shows two different scenarios of forming a RFPM: one is the mirror formed at the rear side of the plasma cavity as proposed in [43] and the other is the mirror formed by a sharp and narrow electron-ion layer driven by the laser pulse [53,59]. One focus, expressed by $\vec{E}_f^+(\rho, t)$ and $\vec{B}_f^+(\rho, t)$, propagates along the $+z$ axis and the other one, expressed by $\vec{E}_f^-(\rho, t)$ and $\vec{B}_f^-(\rho, t)$, along the $-z$ axis. The $+$ and $-$ symbols in the superscripts are used to express the propagating and the counterpropagating RLFs. TM mode laser pulses are assumed in the calculation, so the total fields are expressed as follows:

$$\vec{E}_f^\pm = \gamma \frac{1+\beta}{1-\beta} \frac{\sqrt{\pi}\omega_0 C_f \sqrt{\mathcal{I}_p}}{4cE_{\text{Sch}}} \begin{bmatrix} \{-j_0^\pm \sin(\omega'_0 T^\pm) \Upsilon_1^\pm \pm \beta j_1^\pm \cos(\omega'_0 T^\pm) \Upsilon_2^\pm\} \cos \phi^\pm \\ \{-j_0^\pm \sin(\omega'_0 T^\pm) \Upsilon_1^\pm \pm \beta j_1^\pm \cos(\omega'_0 T^\pm) \Upsilon_2^\pm\} \sin \phi^\pm \\ (1/\gamma) j_0^\pm \sin(\omega'_0 T^\pm) \Upsilon_2^\pm \end{bmatrix} \quad (73a)$$

and

$$\vec{B}_f^\pm = \frac{\gamma}{c} \frac{1+\beta}{1-\beta} \frac{\sqrt{\pi}\omega_0 C_f \sqrt{\mathcal{I}_p}}{4cE_{\text{Sch}}} \begin{bmatrix} -\{\pm j_1^\pm \cos(\omega'_0 T^\pm) \Upsilon_2^\pm - \beta j_0^\pm \sin(\omega'_0 T^\pm) \Upsilon_1^\pm\} \sin \phi^\pm \\ \{\pm j_1^\pm \cos(\omega'_0 T^\pm) \Upsilon_2^\pm - \beta j_0^\pm \sin(\omega'_0 T^\pm) \Upsilon_1^\pm\} \cos \phi^\pm \\ 0 \end{bmatrix}. \quad (73b)$$

Here, $j_i^\pm = j_i(\omega'_0 R^\pm/c)$ and the minus sign in front of j_1^- comes from the change in the sign of the magnetic field. The functions T^\pm and R^\pm for the propagating and counterpropagating RLFs in Eq. (73) are expressed as

$$T^\pm(t, \rho) = \frac{t - (\rho/c)\beta \cos \theta^\pm}{\gamma(1 - \beta^2 \cos^2 \theta^\pm)} \quad (74a)$$

and

$$R^\pm(\rho, t) = \frac{\rho - ct\beta \cos \theta^\pm}{\gamma(1 - \beta^2 \cos^2 \theta^\pm)}. \quad (74b)$$

Since the two RLFs counterpropagate with respect to each other, we find the following relationships for the polar and azimuthal angles between the propagating and the counterpropagating RLFs:

$$\theta^- = \pi - \theta^+ = \pi - \theta \quad \text{and} \quad \phi^- = \phi^+ = \phi. \quad (75)$$

By using Eq. (75), the following relationships for variables between the propagating and counterpropagating RLFs are obtained:

$$T^-(t, \rho) = -T^+(-t, \rho) \quad \text{and} \quad R^-(\rho, t) = R^+(\rho, t), \quad (76a)$$

$$T^-(t, \rho) \pm \frac{R^-(\rho, t)}{c} = -\left[T^+(-t, \rho) \mp \frac{R^+(\rho, -t)}{c} \right], \quad (76b)$$

$$\frac{\sin \theta^-}{\gamma(1 \pm \beta \cos \theta^-)} = \frac{\sin \theta}{\gamma(1 \mp \beta \cos \theta)}, \quad (76c)$$

$$\frac{\cos \theta^- \pm \beta}{1 \pm \beta \cos \theta^-} = -\frac{\cos \theta \mp \beta}{1 \mp \beta \cos \theta}, \quad (76d)$$

and

$$\Upsilon_1^-(t, \rho) = -\Upsilon_1^+(-t, \rho) \quad \text{and} \quad \Upsilon_2^-(t, \rho) = \Upsilon_2^+(-t, \rho). \quad (76e)$$

Thus, the total fields \vec{E}_f^T and \vec{B}_f^T given as the sum of propagating and counterpropagating fields are calculated as

$$\vec{E}_f^T = \vec{E}_f^+ + \vec{E}_f^- = \gamma \frac{1 + \beta}{1 - \beta} \frac{\sqrt{\pi} \omega_0 C_f \sqrt{\mathcal{I}_p}}{4c E_{\text{Sch}}} \begin{bmatrix} -[\mathcal{J}_0(t) + \mathcal{J}_0(-t')] + \beta[\mathcal{J}_1(t) - \mathcal{J}_1(-t')] \cos \phi \\ -[\mathcal{J}_0(t) + \mathcal{J}_0(-t')] + \beta[\mathcal{J}_1(t) - \mathcal{J}_1(-t')] \sin \phi \\ (1/\gamma)[\mathcal{J}'_0(t) - \mathcal{J}'_0(-t')] \end{bmatrix} \quad (77a)$$

and

$$\vec{B}_f^T = \vec{B}_f^+ + \vec{B}_f^- = \frac{\gamma}{c} \frac{1 + \beta}{1 - \beta} \frac{\sqrt{\pi} \omega_0 C_f \sqrt{\mathcal{I}_p}}{4c E_{\text{Sch}}} \begin{bmatrix} -\{[\mathcal{J}_1(t) - \mathcal{J}_1(-t')] - \beta[\mathcal{J}_0(t) + \mathcal{J}_0(-t')]\} \sin \phi \\ \{[\mathcal{J}_1(t) - \mathcal{J}_1(-t')] - \beta[\mathcal{J}_0(t) + \mathcal{J}_0(-t')]\} \cos \phi \\ 0 \end{bmatrix}. \quad (77b)$$

Here, t' is given by $t + t_d$ with a time delay t_d between two fields. The new functions $\mathcal{J}_0(t)$ and $\mathcal{J}_1(t)$ are defined as

$$\mathcal{J}_0(t) = j_0 \left[\frac{\omega'_0 R^+(\rho, t)}{c} \right] \sin[\omega'_0 T^+(t, \rho)] \Upsilon_1^+(t, \rho), \quad (78a)$$

$$\mathcal{J}'_0(t) = j_0 \left[\frac{\omega'_0 R^+(\rho, t)}{c} \right] \sin[\omega'_0 T^+(t, \rho)] \Upsilon_2^+(t, \rho), \quad (78b)$$

and

$$\mathcal{J}_1(t) = j_1 \left[\frac{\omega'_0 R^+(\rho, t)}{c} \right] \cos[\omega'_0 T^+(t, \rho)] \Upsilon_2^+(t, \rho). \quad (78c)$$

Equation (78) has the same form as Eq. (51) with the replacement of field components by the ones superposed with two propagating and counterpropagating RLF fields. In this case, the Poincaré invariants \mathcal{F}^T and \mathcal{G}^T are given by

$$\mathcal{F}^T = \frac{1}{2} \left(\frac{1 + \beta}{1 - \beta} \frac{\sqrt{\pi} \omega_0 C_f \sqrt{\mathcal{I}_p}}{4c} \right)^2 \{ [\mathcal{J}_1(t) - \mathcal{J}_1(-t')]^2 - [\mathcal{J}_0(t) + \mathcal{J}_0(-t')]^2 - [\mathcal{J}'_0(t) - \mathcal{J}'_0(-t')]^2 \} \quad (79a)$$

and

$$\mathcal{G}^T = 0. \quad (79b)$$

The e^+e^- pair production rate W_{ep}^T is calculated as

$$W_{ep}^T \approx 12\pi^2 \alpha \gamma^4 \left(\frac{w_e}{\lambda_0} \right)^2 \left(\frac{\mathcal{I}_p}{\hbar c} \right) [-\mathcal{J}^2(t, t')] \exp \left[-\frac{1}{\gamma^2} \frac{\lambda_0}{w_e} \frac{(E_{\text{Sch}}/E_p)}{\sqrt{6\pi^3} \sqrt{-\mathcal{J}^2(t, t')}} \right], \quad (80)$$

when $\mathcal{F}^T < 0$. In Eq. (80), the function $\mathcal{J}^2(t, t')$ is defined as $[\mathcal{J}_1(t) - \mathcal{J}_1(-t')]^2 - [\mathcal{J}_0(t) + \mathcal{J}_0(-t')]^2 - [\mathcal{J}'_0(t) - \mathcal{J}'_0(-t')]^2$. At $t = 0$, two RLFs overlap at the origin, and \mathcal{F}^T becomes $-2 \times \left(\frac{1 + \beta}{1 - \beta} \frac{\sqrt{\pi} \omega_0 C_f \sqrt{\mathcal{I}_p}}{4c} \right)^2 \mathcal{J}_0^2(0)$. But, in general, it is not necessary for two RLFs to be overlapped at $t = 0$.

The threshold field strength of the incident laser pulse required for a single e^+e^- pair production is examined. In the calculation, two identical RFPMs with a γ -factor of 12.2 are considered with a mirror reflectance of $2.7 \times 10^{-2}\%$ [see Fig. 5(a)]. Due to the beam radius-wavelength ratio, the high harmonic laser pulse is more favorable than the fundamental wavelength of a high-power laser pulse in reducing the threshold required for the pair production. In the numerical calculation of e^+e^- pairs produced, the $\omega'_0 T^\pm(t, \rho)$ and $\omega'_0 R^\pm(\rho, t)$ in Eq. (74) were calculated with $\omega'_0 = \sqrt{(1 + \beta)/(1 - \beta)} \omega_0$. Then, $\mathcal{J}_0(t)$, $\mathcal{J}'_0(t)$, $\mathcal{J}_1(t)$, and $\mathcal{J}^2(t, t')$ in Eqs. (78) and (80) were calculated in series with $\omega'_0 T^\pm(t, \rho)$ and $\omega'_0 R^\pm(\rho, t)$. Next, the e^+e^- pair production rate W_{ep}^T in Eq. (80) was calculated for different time delays.

Figure 5(b) shows the calculated W_{ep}^T at different time delays. Finally, the number of e^+e^- pairs produced for a specific laser [shown in Fig. 5(c)] was obtained after summing up the integrations of W_{ep}^T s over the four-volume obtained for different time delays. The pair production rate is much enhanced in an overlapped volume of two RLFs [see Fig. 5(b)] and the total number of pairs produced in the volume dominates. A time that has the maximal pair production rate for a single RLF is chosen as a proper time delay t_d between two RLFs. For the fourth harmonic Ti:sapphire high power laser pulse, a single e^+e^- pair can be produced at $a_0 = 0.23$ with a γ -factor of 12.2. The characteristic time τ_c for the maximum pulse duration is calculated as about 3.7 fs. This condition can be satisfied by focusing an optical laser pulse (with $\tau_F = 3.5$ fs and a peak power of 0.18 PW at the fourth harmonic wavelength) within a beam radius of 158 μm . By assuming the RFPM with a γ -factor of 12.2 can be driven by focusing a 250 PW laser pulse with a beam radius of 158 μm , this result implies that electron-positron pair production from two colliding RLFs can be expected with a lower laser-power (2×250

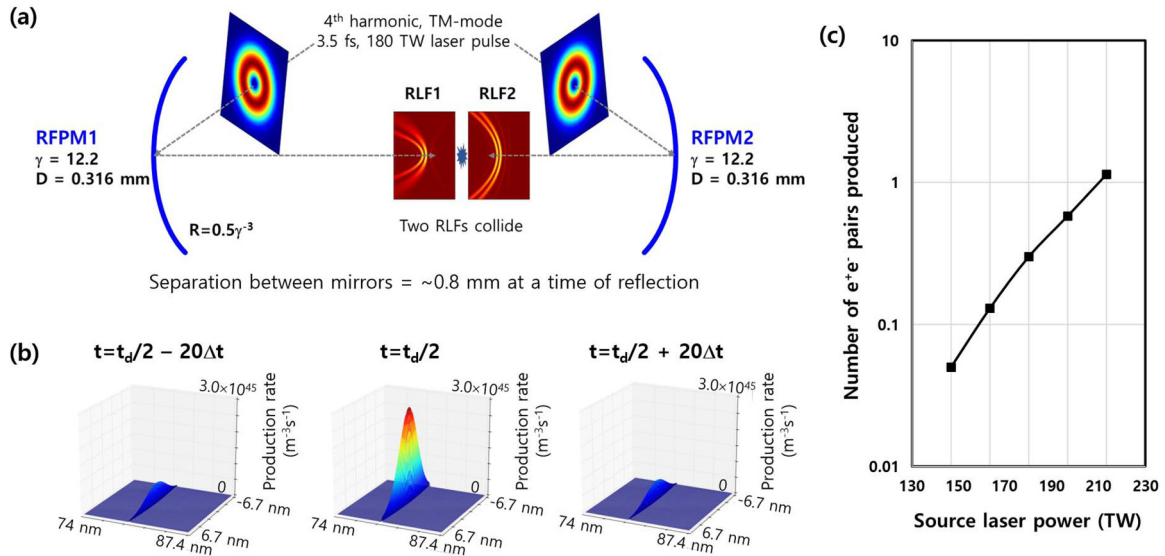


FIG. 5. (a) The e^+e^- pair production by colliding two RLFs. The RFPM is driven by a 250 PW laser pulse and the fourth harmonic laser pulse with a center wavelength of $0.2 \mu\text{m}$ is incident on the RFPM. The diameter D of the mirror is given by $2w_0$. The two RLFs collide with a proper time delay to maximize the pair production. (b) The calculated e^+e^- pair production rate, W_{ep}^T , when two RLFs collide. A strong enhancement in pair production is observed over the overlapped volume at $t = t_d/2$. (c) The number of e^+e^- pairs produced as a function of the source laser power.

PW) laser than that (~ 1000 PW level) calculated under the 4π -spherical focusing condition [24,33]. Again, the determination of characteristic time is based on the one-dimensional model, so the recoil effect in time should be fully understood by a three-dimensional model developed in the near future.

V. CONCLUSION

The mathematical formulas describing the electromagnetic field of the relativistic-flying laser focus formed by an ideal relativistic-flying parabolic mirror were obtained. The main optical characteristics of the relativistic-flying laser focus, such as the enhancement of field strength and its distribution in time and space, could be well understood by the formulas. The field expression of the relativistic-flying laser focus was applied to the estimation of the e^+e^- pair production by the Schwinger mechanism. The pair production rate under the relativistic-flying laser focus was modified by the Lorentz γ -factor and the beam radius-wavelength ratio. The calculation shows that even with a strong suppression due to the low reflectance of the relativistic-flying parabolic mirror, the e^+e^- pair production is feasible by colliding two counterpropagating relativistic-flying laser focuses at a relatively lower laser power of 250 PW. Although we assume an ideal parabolic shape for the relativistic-flying parabolic mirror, the actual

shape of the mirror will have a small deviation from the ideal shape, introducing the wavefront error. The wavefront error deforms the distribution and induces the degradation of the focused intensity. Thus, the next step is to generalize the mathematical formulas for a beam having a wavefront aberration and to calculate the Strehl ratio assessing the focusability. On the other hand, since the formation of the relativistic-flying parabolic mirror will be strongly affected by the instability of the high-power laser pulse and its propagation in the plasma medium, the generation of a stable relativistic-flying parabolic mirror will be a technical challenge for practical applications of the flying mirror. The results obtained can be used to understand the fundamental question of the electron-positron pair production from vacuum.

ACKNOWLEDGMENTS

The work was supported by the project High Field Initiative (Grant No. CZ.02.1.01/0.0/0.0/15_003/0000449) from the European Regional Development Fund. S.S.B. acknowledges support from the U.S. Department of Energy Office of Science Offices of HEP and FES (through LaserNetUS), under Contract No. DE-AC02-05CH11231. T.Z.E., J.K.K., A.S.P., and M.K. acknowledge support from JSPS KAKENHI Grant No. JP19H00669 and QST President's Strategic Grant (Creative Research) No. 20.

- [1] D. Strickland and G. Mourou, *Opt. Commun.* **56**, 219 (1985).
- [2] J. H. Sung, S. K. Lee, T. J. Yu, T. M. Jeong, and J. Lee, *Opt. Lett.* **35**, 3021 (2010).
- [3] ELI-beamlines, <https://www.eli-beams.eu/> (unpublished).
- [4] G. A. Mourou, T. Tajima, and S. V. Bulanov, *Rev. Mod. Phys.* **78**, 309 (2006).
- [5] M. Marklund and P. K. Shukla, *Rev. Mod. Phys.* **78**, 591 (2006).

- [6] E. Esarey, C. B. Schroeder, and W. P. Leemans, *Rev. Mod. Phys.* **81**, 1229 (2009).
- [7] G. V. Dunne, *Eur. Phys. J. D* **55**, 327 (2009).
- [8] A. DiPiazza, C. Muller, K. Z. Hatsagortsyan, and C. H. Keitel, *Rev. Mod. Phys.* **84**, 1177 (2012).
- [9] T. G. Blackburn, D. Seipt, S. S. Bulanov, and M. Marklund, *Phys. Plasma* **25**, 083108 (2018).

- [10] J. J. Klein and B. P. Nigam, *Phys. Rev.* **135**, B1279 (1964).
- [11] F. Karbstein, H. Gies, M. Reuter, and M. Zepf, *Phys. Rev. D* **92**, 071301(R) (2015).
- [12] F. D. Valle, A. Ejlli, U. Gastaldi, G. Messineo, E. Milotti, R. Pengo, G. Ruoso, and G. Zavattini, *Eur. Phys. J. C* **76**, 24 (2016).
- [13] B. Shen, Z. Bu, J. Xu, T. Xu, L. Ji, R. Li, and Z. Xu, *Plasma Phys. Control. Fusion* **60**, 044002 (2018).
- [14] R. Karplus and M. Neuman, *Phys. Rev.* **80**, 380 (1950).
- [15] R. Karplus and M. Neuman, *Phys. Rev.* **83**, 776 (1951).
- [16] B. D. Tollis, *Nuovo Cim.* **32**, 757 (1964).
- [17] B. D. Tollis, *Nuovo Cim.* **35**, 1182 (1965).
- [18] E. Lundström, G. Brodin, J. Lundin, M. Marklund, R. Bingham, J. Collier, J. T. Mendonca, and P. Norreys, *Phys. Rev. Lett.* **96**, 083602 (2006).
- [19] S. V. Bulanov, T. Zh. Esirkepov, Y. Hayashi, M. Kando, H. Kiriya, J. K. Koga, K. Kondo, H. Kotaki, A. S. Pirozhkov, S. S. Bulanov, A. G. Zhidkov, P. Chen, D. Neely, Y. Kato, N. B. Narozhny, and G. Korn, *Nucl. Instrum. Methods Phys. Res. A* **660**, 31 (2011).
- [20] J. K. Koga, S. V. Bulanov, T. Zh. Esirkepov, A. S. Pirozhkov, M. Kando, and N. N. Rosanov, *Phys. Rev. A* **86**, 053823 (2012).
- [21] T. M. Jeong, S. V. Bulanov, P. V. Sasorov, G. Korn, J. K. Koga, and S. S. Bulanov, *Phys. Rev. A* **102**, 023504 (2020).
- [22] J. Schwinger, *Phys. Rev.* **82**, 664 (1951).
- [23] S. S. Bulanov, V. D. Mur, N. B. Narozhny, J. Nees, and V. S. Popov, *Phys. Rev. Lett.* **104**, 220404 (2010).
- [24] A. Gonoskov, I. Gonoskov, C. Harvey, A. Ilderton, A. Kim, M. Marklund, G. Mourou, and A. Sergeev, *Phys. Rev. Lett.* **111**, 060404 (2013).
- [25] J. Q. Yu, H. Y. Lu, T. Takahashi, R. H. Hu, Z. Gong, W. J. Ma, Y. S. Huang, C. E. Chen, and X. Q. Yan, *Phys. Rev. Lett.* **122**, 014802 (2019).
- [26] SULF, <http://english.siom.cas.cn/> (unpublished).
- [27] XCELS, <https://xcels.ipfran.ru/> (unpublished).
- [28] C. N. Danson, C. Haefner, J. Bromage, T. Butcher, J.-C. F. Chanteloup, E. A. Chowdhury, A. Galvanauskas, L. A. Gizzi, J. Hein, D. I. Hillier *et al.*, *High Power Laser Sci. Eng.* **7**, e54 (2019).
- [29] Z. Li, Y. Kato, and J. Kawanaka, *Sci. Rep.* **11**, 151 (2021).
- [30] S. Bahk, P. Rousseau, T. Planchon, V. Chvykov, G. Kalintchenko, A. Maksimchuk, G. Mourou, and V. Yanovsky, *Opt. Lett.* **29**, 2837 (2004).
- [31] T. M. Jeong, S. Weber, B. L. Garrec, D. Margarone, T. Mocek, and G. Korn, *Opt. Express* **23**, 11641 (2015).
- [32] I. Gonoskov, A. Aiello, S. Heugel, and G. Leuchs, *Phys. Rev. A* **86**, 053836 (2012).
- [33] T. M. Jeong, S. V. Bulanov, P. Sasorov, S. S. Bulanov, J. K. Koga, and G. Korn, *Opt. Express* **28**, 13991 (2020).
- [34] V. I. Ritus, *J. Sov. Laser Res.* **6**, 497 (1985).
- [35] D. L. Burke, R. C. Field, G. Horton-Smith, J. E. Spencer, D. Walz, S. C. Berridge, W. M. Bugg, K. Shmakov, A. W. Weidemann, C. Bula, K. T. McDonald, E. J. Prebys, C. Bamber, S. J. Boege, T. Koffas, T. Kotsieroglou, A. C. Melissinos, D. D. Meyerhofer, D. A. Reis, and W. Ragg, *Phys. Rev. Lett.* **79**, 1626 (1997).
- [36] M. Marklund and J. Lundin, *Eur. Phys. J. D* **55**, 319 (2009).
- [37] B. King, H. Hu, and B. Shen, *Phys. Rev. A* **98**, 023817 (2018).
- [38] C. Baumann, E. N. Nerush, A. Pukhov, and I. Y. Kostyukov, *Sci. Rep.* **9**, 9407 (2019).
- [39] A. DiPiazza, M. Tamburini, S. Meuren, and C. H. Keitel, *Phys. Rev. A* **99**, 022125 (2019).
- [40] S. V. Bulanov, T. Zh. Esirkepov, M. Kando, A. S. Pirozhkov, and N. N. Rosanov, *Phys. Usp.* **56**, 429 (2013).
- [41] F. Quere and H. Vincenti, *High Power Laser Sci. Eng.* **9**, e6 (2021).
- [42] A. Einstein, *Ann. Phys.* **17**, 891 (1905).
- [43] S. V. Bulanov, T. Zh. Esirkepov, and T. Tajima, *Phys. Rev. Lett.* **91**, 085001 (2003).
- [44] P. Zhang, S. S. Bulanov, D. Seipt, A. V. Arefiev, and A. G. R. Thomas, *Phys. Plasma* **27**, 050601 (2020).
- [45] M. Kando, A. S. Pirozhkov, K. Kawase, T. Zh. Esirkepov, Y. Fukuda, H. Kiriya, H. Okada, I. Daito, T. Kameshima, Y. Hayashi, H. Kotaki, M. Mori, J. K. Koga, H. Daido, A. Y. Faenov, T. Pikuz, J. Ma, L.-M. Chen, E. N. Ragozin, T. Kawachi *et al.*, *Phys. Rev. Lett.* **103**, 235003 (2009).
- [46] S. V. Bulanov, T. Zh. Esirkepov, M. Kando, and J. Koga, *Plasma Sources Sci. Technol.* **25**, 053001 (2016).
- [47] J. Koga, S. V. Bulanov, T. Zh. Esirkepov, M. Kando, S. S. Bulanov, and A. Pirozhkov, *Plasma Phys. Control. Fusion* **60**, 074007 (2018).
- [48] T. Zh. Esirkepov, J. Mu, Y. Gu, T. M. Jeong, P. Valenta, O. Klimo, J. K. Koga, M. Kando, D. Neely, G. Korn, S. V. Bulanov, and A. S. Pirozhkov, *Phys. Plasmas* **27**, 052103 (2020).
- [49] J. Mu, T. Zh. Esirkepov, P. Valenta, Y. Gu, T. M. Jeong, A. S. Pirozhkov, J. K. Koga, M. Kando, G. Korn, and S. V. Bulanov, *Phys. Rev. E* **102**, 053202 (2020).
- [50] D. H. Froula, D. Turnbull, A. S. Davies *et al.*, *Nat. Photon.* **12**, 262 (2018).
- [51] T. M. Jeong, S. V. Bulanov, S. Weber, and G. Korn, *Opt. Express* **26**, 33091 (2018).
- [52] G. V. Dunne, H. Gies, and R. Schutzhold, *Phys. Rev. D* **80**, 111301(R) (2009).
- [53] A. S. Pirozhkov, J. Ma, M. Kando, T. Zh. Esirkepov, Y. Fukuda, L.-M. Chen, I. Daito, K. Ogura, T. Homma, Y. Hayashi, H. Kotaki, A. Sagisaka, M. Mori, J. K. Koga, T. Kawachi, H. Daido, S. V. Bulanov, T. Kimura, Y. Kato, and T. Tajima, *Phys. Plasma* **14**, 123106 (2007).
- [54] S. V. Bulanov and A. S. Sakharov, *JETP Lett.* **54**, 203 (1991).
- [55] N. H. Matlis, S. Reed, S. S. Bulanov, V. Chvykov, G. Kalintchenko, T. Matsuoka, P. Rousseau, V. Yanovsky, A. Maksimchuk, S. Kalmykov, G. Shvets, and M. C. Downer, *Nat. Phys.* **2**, 749 (2006).
- [56] I. Gradshteyn and I. Ryzhik, *Table of Integrals, Series, and Products* (Elsevier, New York, 2007).
- [57] P. Valenta, T. Zh. Esirkepov, J. K. Koga, A. S. Pirozhkov, M. Kando, T. Kawachi, Y.-K. Liu, P. Fang, P. Chen, J. Mu, G. Korn, O. Klimo, and S. V. Bulanov, *Phys. Plasma* **27**, 032109 (2020).
- [58] V. V. Kulagin, V. A. Cherepenin, M. S. Hur, and H. Suk, *Phys. Plasma* **14**, 113101 (2007).
- [59] T. Zh. Esirkepov, S. V. Bulanov, M. Kando, A. S. Pirozhkov, and A. G. Zhidkov, *Phys. Rev. Lett.* **103**, 025002 (2009).
- [60] V. B. Berestetskii, E. M. Lifshitz, and L. P. Pitaevskii, *Quantum Electrodynamics* (Pergamon, Oxford, 1982).
- [61] N. B. Narozhny, S. S. Bulanov, V. D. Mur, and V. S. Popov, *Phys. Lett. A* **330**, 1 (2004).
- [62] I. A. Aleksandrov, G. Plunien, and V. M. Shabaev, *Phys. Rev. D* **99**, 016020 (2019).